Macroscopic model for unsteady flow in porous media

Didier Lasseux, Francisco J. Valdès-Parada, Fabien Bellet

J. Fluid Mech. (2019), vol. 862, pp. 283-311. doi:10.1017/jfm.2018.878

Macroscopic model for unsteady flow in porous media

Didier Lasseux[1]†, **Francisco J. Valdés-Parada**[2]
Fabien Bellet[3]

[1]CNRS, I2M, UMR 5295
Esplanade des Arts et Métiers, 33405 Talence, Cedex, France.
[2]Universidad Autónoma Metropolitana-Iztapalapa
Departamento de Ingeniería de Procesos e Hidráulica
Av. San Rafael Atlixco 186, 09340 Ciudad de México, Mexico.
[3]Laboratoire EM2C, CNRS, CentraleSupélec, Université Paris-Saclay
3, rue Joliot Curie, 91192 Gif-sur-Yvette Cedex, France.

(Accepted 28 October 2018)

The present article reports on a formal derivation of a macroscopic model for unsteady one-phase incompressible flow in rigid and periodic porous media using an upscaling technique. The derivation is carried out in the time domain in the general situation where inertia may have a significant impact. The resulting model is non-local in time and involves two effective coefficients in the macroscopic filtration law, namely a dynamic apparent permeability tensor, $\mathbf{H}_t$, and a vector, $\boldsymbol{\alpha}$, accounting for the time-decaying influence of the flow initial condition. This model generalizes previous non-local macroscale models restricted to creeping flow conditions. Ancillary closure problems are provided, which allow computing the effective coefficients. Symmetry and positiveness analyses of $\mathbf{H}_t$ are carried out, evidencing that this tensor is symmetric only in the creeping regime. The effective coefficients are functions of time, geometry, macroscopic forcings and the initial flow condition. This is illustrated through numerical solutions of the closure problems. Predictions are made on a simple periodic structure for a wide range of Reynolds numbers smaller than the critical value characterizing the first Hopf bifurcation. Finally, the performance of the macroscopic model for a variety of macroscopic forcing and initial conditions is examined in several case studies. Validation through comparisons with direct numerical simulations is performed. It is shown that the purely heuristic classical model, widely used for unsteady flow, consisting in a Darcy-like model complemented with an accumulation term on the filtration velocity, is inappropriate.

1. Introduction

Unsteady flow in porous media has been the subject of active research over, at least, the past sixty years. One of the main interests has been the propagation of acoustic waves in porous structures with applications in seismic waves, enhanced oil recovery, ocean bottom interactions and coastal waves, superfluid flow in porous media, among many others, in addition to the fundamental nature of deriving appropriate physical models. This was initiated by the pioneer works from Biot (1956*a*,*b*) to analyze effects such as wave speed, attenuation, viscous dissipation and anisotropy. An overview of the literature on the subject may lead to classify studies into three main groups, namely studies about elastic media without any fluid external forcing, studies of time-dependent flow in rigid porous media and fluid flow through elastic media. In the present work,

† Email address for correspondence: didier.lasseux@u-bordeaux.fr

the interest is focused upon incompressible and unsteady single-phase flow through rigid homogeneous periodic porous media. Existing reported works may be conveniently summarized by distinguishing those carried out in the time-domain from those developed in the frequency-domain. In the following paragraphs a non-exhaustive literature review of both branches is presented.

Description of unsteady incompressible one-phase flow in porous media has been widely relying on extensions to the steady version of Darcy's law, or, when inertia is taken into account, to the Darcy-Forchheimer corrected form. To the best of our knowledge, one of the earliest extensions to account for unsteady effects was put forth by Polubarinova-Kochina (1962). In this work, an acceleration term on the filtration velocity was kept in the macroscopic momentum equation as obtained from a direct analogy with the Stokes (or Navier-Stokes) equation in which the point velocity is replaced by the average velocity and the external force by the average friction on the solid surface of the porous matrix, *i.e.* the Darcy term. Despite its lack of rigorous formal derivation, this type of approach has been considered as a valid one and became classical over the past half century (Rajagopal 2007; Bories *et al.* 2008; Nield & Bejan 2013). This model will be referred to as the "*heuristic model*". It has been widely used, for instance, in numerical simulations (Dogru *et al.* 1978), for stability analysis of fluid-flow between an impermeable plate an a porous wall (Hill & Straughan 2008, 2009) or for turbulence in a similar configuration (Breugem *et al.* 2006) or in a confined porous medium (Jin & Kuznetsov 2017) as well as for three-dimensional stability analysis of flow between two parallel porous walls (Tilton & Cortelezzi 2008); for the analysis of forced or natural convection in porous media (Kuznetsov & Nield 2006); the transition to chaos in natural convection (Vadasz 1999), among many other applications. Few formal analyses were dedicated to tentatively derive the heuristic model and some of them may have been inspired by the development of the steady macroscopic model of one-phase flow in porous media including inertia by Whitaker (1996). In fact, in this reference, the acceleration term was kept in a large part of the development although it was clearly stated, at the final stage, that the steady ancillary closure problem used to derive the closed average model was only compatible with a steady version of this model (see section 2.8 in this reference). However, the unsteady version of this model was used by Tilton & Cortelezzi (2008) with a reference to Whitaker (1996). Two other works (Teng & Zhao 2000; Breugem *et al.* 2006) proposed a development yielding the unsteady form of the macroscopic model developed by Whitaker (1996) (equation (2.26)) that, indeed, corresponds to the heuristic model. However, in these works, the closure procedure is not considered and the time-scale constraint is not addressed. Nevertheless, in a recent paper, Zhu *et al.* (2014) further considered this version of the unsteady model and showed, from comparison with direct numerical simulation (DNS), that it was inappropriate. With the sake of keeping the same form of the unsteady model, the acceleration term was modified by conveniently introducing a time constant obtained by averaging the energy equation, an idea that was employed by Laushey & Popat (1968) to interpret results obtained on model unconfined aquifers. Comparisons with DNS results showed agreement. However, this time constant requires knowledge of the pore-scale flow field featuring a non-closed overall model that can not be used as a predictive one even under creeping flow conditions.

The approach making use of the heuristic model has been also very popular in wave dampening models in coastal engineering (Hall *et al.* 1995; Corvaro *et al.* 2010). In this field, however, the lack of accuracy of the approach, compared to experimental data, led numerous authors to modify the heuristic model by affecting a premultiplying factor, usually called "*inertial coefficient*", to the accumulation term. Without any formal derivation, this was justified by an analogous concept of an added virtual mass force

used for modelling flow around an isolated obstacle. This concept was first introduced by Sollitt & Cross (1972) and many different forms of the inertial coefficient were proposed since then (see a short review in Burcharth & Andersen (1995)). A formal derivation of this modified version of the heuristic model was attempted (Abderahmane *et al.* 2002) but the development suffers again, at the final stage, from a formal identification of the macroscopic model to be obtained with the microscopic model. The misleading use of the heuristic model was pointed out by Auriault (1999) indicating that the macroscopic momentum equation should contain a memory effect expressed by a convolution product between the filtration velocity and a memory function. The proof of this form was anticipated by the same author (Auriault 1980), and almost simultaneously by Lions (1981). It was later reconsidered by Allaire (1992), Mikelić (1994) and more recently in Mei & Vernescu (2010) (the term "*permeability*" attributed to the memory function in the latter references is inadequate as it is dimensionally incorrect). However, as will be commented in the following sections, the reported developments require to be completed, either by taking into account the initial condition or by explicitly providing the closure problems yielding the effective coefficients, in particular in the case where inertia is significant. Upscaling the Navier-Stokes (or Euler) equations was also addressed using the homogenization technique (Sanchez-Palencia 1980; Masmoudi 1998, 2002; Lions & Masmoudi 2005). However, as will be further commented in section 3.2, no complete unsteady macroscopic model was reported with this technique. Some other derivations were reported in the literature, mainly developed in the Fourier domain.

Regarding the literature about unsteady flow modelling in porous media in the frequency domain, it is worth mentioning that one serious drawback of early Biot's theory lies in the lack of providing numerical predictions of the effective medium coefficients involved in the macroscale model. This issue was addressed by Auriault *et al.* (1985) who used the homogenization technique to derive a Darcy-law type model to describe unsteady creeping flow in rigid and deformable porous media, assuming the fluid to be at rest in the porous matrix as the initial condition. Predictions of the model were validated with experimental results. This study is a continuation of previous works by Lévy (1979) and Auriault (1980), where the homogenization method was used to study flow through elastic porous media. In the work by Lévy, the resulting expression is also a Darcy-law type model in the frequency domain, while the work by Auriault is an extension to include inertial effects and multiphase flow. This upscaling approach was also used by Sheng & Zhou (1988) (see also Zhou & Sheng (1989)) to predict the dynamic permeability as a function of frequency for a variety of microstructures in the creeping flow regime. These authors proposed to scale the predicted dynamic permeability, $\kappa(\omega)$, by its static value, κ_0, in order to produce a universal curve independent of the microstructure when plotted against a scaled frequency (ω_c) that is particular of the microscale geometry and flow properties. In this way, these authors proposed the following empirical relationship

$$\frac{\kappa(\omega)}{\kappa_0} = f\left(\frac{\omega}{\omega_c}\right) \tag{1.1}$$

with f being a so-called universal structure function independent of the microstructure. Later on, Charlaix *et al.* (1988) reported experimental measurements of the dynamic permeability on capillary tubes and model porous media made of fused glass beads and crushed glass of different sizes for conditions in which the flow was in the transition between the creeping and inertial regimes. These authors found that their experimental measurements were in agreement with the relationship proposed by Sheng & Zhou (1988). However, their experiments were performed on samples featuring a rather narrow range of topology varieties. A few time later, Johnson (1989) proposed an ana-

lytical expression for f, which is given not only in terms of ω_c, but also of a parameter $M = 8\alpha_\tau\kappa_0/\varepsilon\Lambda^2$, with α_τ, ε and Λ being the tortuosity factor, the porosity and a characteristic length that was taken to be twice the pore volume to surface ratio (Johnson *et al.* 1987), respectively.

Advances in numerical capabilities made possible predictions of the dynamics of the permeability in more complex geometries than those used before. In this regard, Chapman & Higdon (1992) solved the unsteady version of the Stokes problem in several three-dimensional periodic unit cells. The resulting average velocity was used in the unsteady version of Darcy's law in the frequency domain to predict the dynamic permeability. In order to emphasize porosity and frequency effects, the permeability dependence upon frequency was not represented in the universal curve suggested above. In the same year, Smeulders *et al.* (1992) reported numerical simulations and experimental measurements that corroborated the universal relationship proposed by Sheng & Zhou (1988) when more parameters are considered in the structure function. In addition, these authors rigorously derived the analytical relationship proposed by Johnson *et al.* (1987) using the homogenization technique. Departures from the relationship given in equation (1.1) were reported by Achdou & Avellaneda (1992) for microgeometries consisting of corrugated tubes. These authors observed a slower convergence of the dynamic permeability towards its steady state value than that predicted by the empirical relationship. This issue was later addressed by Cortis *et al.* (2003), who used direct numerical simulations to show that the predictions from the relationship in equation (1.1) are justified for microchannels with corrugated, and even wedge-shaped, walls. In the present work, the issue of the universality of the above mentioned empirical relation is not going to be further discussed.

The purpose of this article is to carry out a careful derivation of the macroscopic unsteady model for one-phase flow in rigid and periodic porous media including inertial effects and taking into account the influence of the initial flow condition. This is achieved by upscaling the unsteady solution of the initial boundary value problem operating at the pore-scale using a short-cut version of the volume averaging technique, which has the nice feature to lead to a closure scheme for the prediction of the corresponding effective medium coefficients. The developments detailed hereafter are organized as follows. After recalling the pore-scale model in section 2, the upscaling procedure is detailed in section 3. The development is performed in the time-domain yielding the unsteady macroscopic model which involves the time rate of change of the convolution product between the dynamic apparent permeability tensor, $\mathbf{H}_t$, and the macroscopic pressure gradient, as well as an effective vectorial term, $\boldsymbol{\alpha}$, which accounts for the effect of the initial condition. The two effective coefficients $\mathbf{H}_t$ and $\boldsymbol{\alpha}$ can be computed from the solution of two time-dependent closure problems that are explicitly provided. This general model encompasses the special case of creeping flow. Symmetry and positiveness properties of the dynamic apparent permeability tensor are investigated. In addition, illustrative examples of the dynamics of the effective coefficients are provided. Section 4 is dedicated to results obtained for a model periodic porous structure involving four stiff case studies, which serve as tests of the performance of the upscaled and heuristic models with respect to direct numerical simulations. Concluding remarks are presented in section 5.

2. Pore-scale model

The development starts with the classical mass and momentum Navier-Stokes equations describing flow of a single Newtonian and incompressible fluid phase β that saturates the void space of a porous medium whose skeleton is made of a non deformable solid phase σ such as the one sketched in figure 1a. At any point in the pore-space occupied

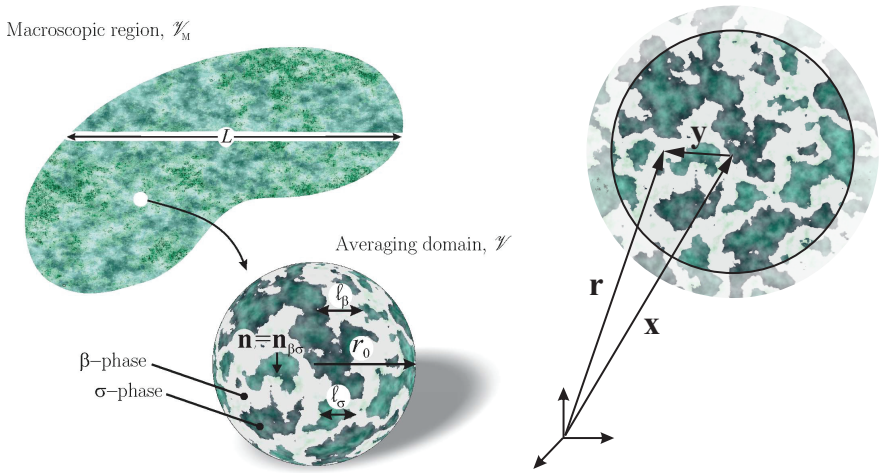

FIGURE 1. a) Sketch of a porous medium including a sample of the averaging volume and the characteristic length-scales. $\mathscr{V}_M$ denotes the entire domain composed of the homogeneous part ($\mathscr{V}_{Mh}$) and the region near the boundary ($I(\partial\mathscr{V}_M)$), *i.e.* $\mathscr{V}_M = \mathscr{V}_{Mh} \cup I(\partial\mathscr{V}_M)$. b) Position vectors associated to the averaging volume.

by the β-phase, $\mathscr{V}_{\beta,M}$, and at any instant, these equations are given by

$$\nabla \cdot \mathbf{v}_{\beta M} = 0, \quad \text{in} \quad \mathscr{V}_{\beta,M}, t > 0 \tag{2.1a}$$

$$\rho\left(\frac{\partial \mathbf{v}_{\beta M}}{\partial t} + \mathbf{v}_{\beta M} \cdot \nabla \mathbf{v}_{\beta M}\right) = -\nabla p_{\beta M} + \rho\mathbf{b} + \mu\nabla^2 \mathbf{v}_{\beta M}, \quad \text{in} \quad \mathscr{V}_{\beta,M}, t > 0 \tag{2.1b}$$

where $p_{\beta M}$ and $\mathbf{v}_{\beta M}$ are the fluid pressure and velocity, respectively; t denotes time, $\rho\mathbf{b}$ is the body force per unit volume, $\mathbf{b}$ being space-independent (but eventually time-varying) while ρ and μ represent the density and dynamic viscosity of the fluid, respectively, which are considered constants. Furthermore, the no-slip boundary condition is enforced at the fixed solid-fluid interface, $\mathscr{A}_{\beta\sigma,M}$

$$\mathbf{v}_{\beta M} = \mathbf{0}, \quad \text{at} \quad \mathscr{A}_{\beta\sigma,M}, t \geqslant 0 \tag{2.1c}$$

In addition, the velocity at the macroscopic boundaries, $\mathscr{A}_{\beta,M}$, is assumed to be known and can be expressed as

$$\mathbf{v}_{\beta M} = \mathbf{v}_{in} \text{ or } p_{\beta M} = p_{in}, \quad \text{at} \quad \mathscr{A}_{\beta,M}, t > 0 \tag{2.1d}$$

Finally, the corresponding initial condition is given by

$$\mathbf{v}_{\beta M} = \mathbf{v}_0, \quad \text{when} \quad t = 0, \quad \text{in} \quad \mathscr{V}_{\beta,M} \tag{2.1e}$$

It is worth mentioning that, in general, measurements of $\mathbf{v}_{in}$ (or p_{in}) and $\mathbf{v_0}$ are not easily obtained but, nonetheless, for the development that follows, it is assumed that this information is available. However, as it will be shown in the next paragraphs, not all of this information is actually required in the final upscaled model.

3. Averaging

On the basis of the above stated initial boundary value problem, the purpose of the analysis is to derive a macroscopic unsteady flow model including inertia. To this

end, an upscaling procedure must be applied. Among techniques like homogenization (Auriault *et al.* 2009) or the Thermodynamically Constrained Averaging Technique (Gray & Miller 2014) and many others (Cushman *et al.* 2002), the method of volume averaging (Whitaker 1999) is retained in this work. In order to spatially smooth the pore-scale heterogeneities, it is necessary to introduce an averaging operator, which can be applied to the field of any piece-wise continuous function, ψ, defined everywhere in the β-phase as

$$\langle \psi \rangle|_{\mathbf{x},t} = \frac{1}{V} \int\limits_{\mathscr{V}_\beta(\mathbf{x})} \psi(\mathbf{r},t)\, dV \tag{3.1a}$$

where the position vector $\mathbf{x}$ locates the centroid of the averaging domain, whereas $\mathbf{y}$ and $\mathbf{r} = \mathbf{y}+\mathbf{x}$ locate points within the β-phase with respect to $\mathbf{x}$ and a fixed coordinate system, respectively, as indicated in figure 1b. In the above expression $\mathscr{V}$, denotes the averaging volume of measure V and radius r_0 (see figure 1a). The averaging operator defined in equation (3.1*a*) is usually denoted as the superficial averaging operator (Whitaker 1999), a nomenclature that is employed throughout the article. In addition, the intrinsic averaging operator is defined as

$$\langle \psi \rangle^\beta\big|_{\mathbf{x},t} = \frac{1}{V_\beta(\mathbf{x})} \int\limits_{\mathscr{V}_\beta(\mathbf{x})} \psi(\mathbf{r},t)\, dV \tag{3.1b}$$

where $V_\beta(\mathbf{x})$ represents the volume of the β-phase within $\mathscr{V}$. The superficial and intrinsic averaging operators are related by the Dupuit-Forchheimer relationship

$$\langle \psi \rangle|_{\mathbf{x},t} = \varepsilon(\mathbf{x})\, \langle \psi \rangle^\beta\big|_{\mathbf{x},t} \tag{3.2}$$

with $\varepsilon(\mathbf{x}) \equiv V_\beta(\mathbf{x})/V$ denoting the porosity which is a constant due to the rigid and homogeneous character of the medium. To facilitate the notation, subscripts $\mathbf{x}$ and t will be omitted in the remainder of the article.

While carrying out the analysis, the general transport theorem (Truesdell & Toupin 1960; Slattery 1999) and the spatial averaging theorem (Howes & Whitaker 1985) will be employed. They are respectively given by

$$\left\langle \frac{\partial \psi}{\partial t} \right\rangle = \frac{\partial \langle \psi \rangle}{\partial t} - \frac{1}{V} \int\limits_{\mathscr{A}_{\beta\sigma}} \mathbf{n} \cdot \mathbf{w} \psi\, dA \tag{3.3a}$$

$$\langle \nabla \psi \rangle = \nabla \langle \psi \rangle + \frac{1}{V} \int\limits_{\mathscr{A}_{\beta\sigma}} \mathbf{n} \psi\, dA \tag{3.3b}$$

In the equations above, $\mathbf{n}$ is the unit normal vector at $\mathscr{A}_{\beta\sigma}$ directed from the β-phase towards the σ-phase as indicated in figure 1a and $\mathbf{w}$ denotes the displacement velocity of $\mathscr{A}_{\beta\sigma}$. Because the porous medium is assumed to be rigid, $\mathbf{w} = \mathbf{0}$ and, together with the fact the structure is homogeneous, the above theorems may be rewritten in terms of intrinsic averages as follows

$$\left\langle \frac{\partial \psi}{\partial t} \right\rangle^\beta = \frac{\partial \langle \psi \rangle^\beta}{\partial t} \tag{3.4a}$$

$$\langle \nabla \psi \rangle^\beta = \nabla \langle \psi \rangle^\beta + \frac{1}{V_\beta} \int\limits_{\mathscr{A}_{\beta\sigma}} \mathbf{n} \psi\, dA \tag{3.4b}$$

As for any upscaling technique, a scale hierarchy is assumed as a prerequisite, namely a separation of characteristic length-scales that can be stated as

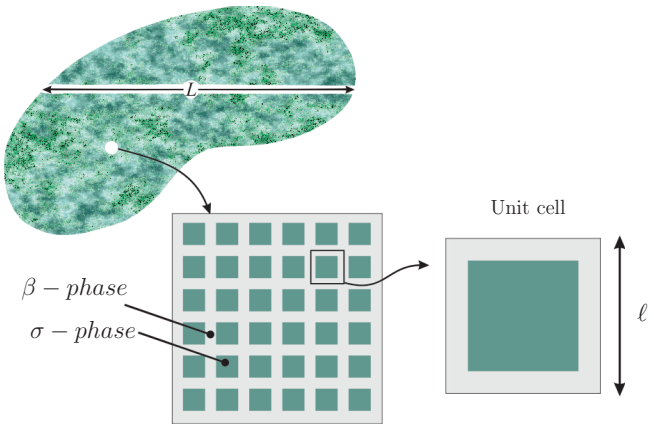

FIGURE 2. Two-dimensional sketch of a periodic structure and a geometrical periodic unit cell of side length ℓ.

$$\ell_\beta \ll r_0 \ll L \tag{3.5}$$

where ℓ_β represents the characteristic pore length-scale and L the size of the macroscopic domain.

In order to derive a model that is expressed only in terms of macroscopic quantities, it is convenient to introduce the following spatial decomposition (Gray 1975)

$$\psi = \langle\psi\rangle^\beta + \tilde{\psi}, \quad \psi = \mathbf{v}, p \tag{3.6}$$

This decomposition is intended to operate a spatial length-scale decoupling as the deviation field, $\tilde{\psi}$, is expected to vary at the scale ℓ_β while the intrinsic average, $\langle\psi\rangle^\beta$, experiences significant variations at the scale L. This contrast can be clearly established at steady-state and, for the dynamic flow process under consideration, it is assumed that this condition is satisfied at any time. As a consequence of the scale hierarchy expressed in (3.5), $\langle\psi\rangle^\beta$ can be treated as a constant at all times within the averaging volume (Whitaker 1999), with the consequence that

$$\langle\tilde{\psi}\rangle^\beta \simeq 0 \tag{3.7}$$

The development of the macroscopic model is now carried out considering that the porous medium is periodic, which represents a classical hypothesis in upscaling methods. Under these circumstances, it is sufficient to consider the above stated initial boundary value problem (equations (2.1)) over a periodic unit cell that will be corresponding to the averaging volume $\mathscr{V}$. Here, special attention should be paid to the fact that, for unsteady flow, this periodic unit cell may not necessarily coincide with the geometrical one depicted in figure 2. This was highlighted in the study of the first Hopf bifurcation in model periodic structures in the work by Agnaou *et al.* (2016).

3.1. *Formal solution in a unit cell*

With the above materials at disposal, the analysis can be directed to the homogeneous part $\mathscr{V}_{Mh}$ of the entire domain, *i.e.* excluding the region $I(\partial\mathscr{V}_M)$ near the macroscopic boundary of the system. A development similar to that reported by Whitaker (1996) may be followed to reach a macroscopic model involving only the average velocity and pressure. However, following the idea used in section 2 of the article by Barrere *et al.* (1992), a shorter alternative procedure, which basically consists in expressing the formal solution

of the pore-scale initial boundary value problem over a periodic unit cell in terms of the driving forces, followed by an averaging step, may be adopted to considerably simplify the development. The use of periodicity is more a convenience than a necessity, since the same procedure can be adopted without this restriction. This approach is consistent with the assumption of separation of length-scales in the homogeneous region of the porous medium. With this purpose in mind, the pore-scale problem in equations (2.1) is re-written in a periodic unit cell in terms of the dependent variables $\mathbf{v}$ and p. Unlike $\mathbf{v}$, p is not a periodic field but the decomposition provided in equation (3.6) shall be used so that $\tilde{p}$ is periodic, yielding

$$\nabla \cdot \mathbf{v} = 0, \quad \text{in} \quad \mathscr{V}_\beta, t > 0 \tag{3.8a}$$

$$\rho\left(\frac{\partial \mathbf{v}}{\partial t} + \mathbf{v}\cdot\nabla\mathbf{v}\right) = -\nabla\tilde{p} + \mu\nabla^2\mathbf{v} + \underbrace{\left(-\nabla\langle p\rangle^\beta + \rho\mathbf{b}\right)}_{source}, \quad \text{in} \quad \mathscr{V}_\beta, t > 0 \tag{3.8b}$$

$$\mathbf{v} = \mathbf{0}, \quad \text{at} \quad \mathscr{A}_{\beta\sigma}, t \geqslant 0 \tag{3.8c}$$

$$\mathbf{v} = \underbrace{\mathbf{v}_0}_{source}, \quad \text{in} \quad \mathscr{V}_\beta, \quad \text{when} \quad t = 0 \tag{3.8d}$$

$$\langle\tilde{p}\rangle^\beta = 0, \qquad t > 0 \tag{3.8e}$$

$$\mathbf{v}(\mathbf{r}+\mathbf{l}_i) = \mathbf{v}(\mathbf{r}); \quad \tilde{p}(\mathbf{r}+\mathbf{l}_i) = \tilde{p}(\mathbf{r}), \quad t > 0, \quad i = 1,2,3 \tag{3.8f}$$

where $\mathscr{V}_\beta$ and $A_{\beta\sigma}$ respectively designate the region occupied by the β-phase and the solid-fluid interface within the unit cell of periodic lattice vectors $\mathbf{l}_i$. Notice that equations (3.8*e*) and (3.8*f*) replace the external boundary condition in equation (2.1*d*).

The nonlinear character of the above problem makes a formal solution very difficult to obtain and, for this reason, a linearization approach is of interest. Indeed, a solution at time t can be sought assuming that the convective velocity exists and is available at a time $t-\Delta t$, for any small enough value of Δt. Under these circumstances, the momentum equation (3.8*b*) can be approximated using a $0th$ order Taylor expansion in time, leading to the approximation $\mathbf{v}|_t \approx \mathbf{v}|_{t-\Delta t} \equiv \mathbf{v}_\Delta$. In this way, equation (3.8*b*) takes the form

$$\rho\left(\frac{\partial \mathbf{v}}{\partial t} + \mathbf{v}_\Delta\cdot\nabla\mathbf{v}\right) = -\nabla\tilde{p} + \mu\nabla^2\mathbf{v} + \underbrace{\left(-\nabla\langle p\rangle^\beta + \rho\mathbf{b}\right)}_{source}, \quad \text{in} \quad \mathscr{V}_\beta, t > 0 \tag{3.9}$$

This type of approximation is a consistent one and is typical in a numerical approach consisting of a linearization of the convective term that makes use of an explicit form of the convective velocity. As it will be shown later, the information about the time step and the rest of the terms of the Taylor expansion in time are ultimately not required in the resulting closure problems. With the momentum balance in the form of equation (3.9), the initial and boundary-value problem is a linear one for which a formal solution can be obtained using an integral equation formulation in terms of Green's functions as shown by Wood & Valdés-Parada (2013). This solution can be written as

$$\mathbf{v} = \frac{1}{\mu}\left(\frac{\partial \mathbf{D}}{\partial t} * \cdot\left(-\nabla\langle p\rangle^\beta + \rho\mathbf{b}\right) + \mathbf{m}_0\right), \quad \text{in} \quad \mathscr{V}_\beta, t > 0 \tag{3.10a}$$

$$\tilde{p} = \frac{\partial \mathbf{d}}{\partial t} * \cdot\left(-\nabla\langle p\rangle^\beta + \rho\mathbf{b}\right) + n_0, \quad \text{in} \quad \mathscr{V}_\beta, t > 0 \tag{3.10b}$$

In these two equations, as in the remainder of the article, the notation $*\cdot$ is adopted to denote the combined convolution and dot products. For two time-dependent tensors of

any order, $\boldsymbol{\kappa}_1$ and $\boldsymbol{\kappa}_2$, this product is given by

$$\boldsymbol{\kappa}_1 * \cdot \boldsymbol{\kappa}_2 = \int_{t_0=0}^{t_0=t} \boldsymbol{\kappa}_1|_{t-t_0} \cdot \boldsymbol{\kappa}_2|_{t_0}\, dt_0 = \int_{t_0=0}^{t_0=t} \boldsymbol{\kappa}_1|_{t_0} \cdot \boldsymbol{\kappa}_2|_{t-t_0}\, dt_0 \tag{3.11}$$

While writing the representations in equations (3.10), it is meant that $\partial\mathbf{D}/\partial t$ (respectively $\partial\mathbf{d}/\partial t$) is the closure variable that maps $\left(-\nabla\langle p\rangle^{\beta} + \rho\mathbf{b}\right)$ onto $\mathbf{v}$ (respectively $\tilde{p}$) while $\mathbf{m}_0$ (respectively n_0) is the closure variable that maps $\mathbf{v}_0$ onto $\mathbf{v}$ (respectively $\tilde{p}$). At this point, it is worth mentioning that the initial conditions for $\mathbf{D}$ and $\mathbf{d}$ yield unique solutions that are driven by the sources as it will be provided later in the derivations.

It must be mentioned that the formal solution given in equations (3.10) does not correspond, except when $\mathbf{v}_0 = \mathbf{0}$, to the one reported by Lions (1981) (see equation (5.20) therein), under creeping flow conditions, and by Mikelić (1994) (see equation (P) for the creeping regime solution and the "Proof of Theorem 1.4" in section 2.4, for the inertial case solution in the Laplace domain, therein). The difference lies in the fact that these authors considered the initial condition to be a function only of $\mathbf{x}$ as proposed in equation (5.10) of Chapter 2 in Lions (1981). Notice that this assumption is physically questionable and it is not retained in the present work just as it was not considered by Allaire (1992) for the study of unsteady creeping flow in porous media.

The macroscopic mass and momentum conservation equations can now be obtained by applying the superficial averaging operator on equations (3.8*a*) and (3.10*a*), respectively. In order to obtain the macroscale mass conservation equation, it is also necessary to make use of the averaging theorem, together with the no slip boundary condition, leading to

$$\nabla \cdot \langle \mathbf{v} \rangle = 0, \quad \text{in } \mathscr{V}_{Mh},\ t > 0 \tag{3.12a}$$

In addition, the macroscale filtration velocity equation is given by

$$\langle \mathbf{v} \rangle = -\frac{1}{\mu}\left(\frac{\partial\langle \mathbf{D}\rangle}{\partial t} * \cdot \left(\nabla\langle p\rangle^{\beta} - \rho\mathbf{b}\right) - \langle \mathbf{m}_0 \rangle\right), \quad \text{in } \mathscr{V}_{Mh},\ t > 0 \tag{3.12b}$$

Here, the assumption that $\nabla\langle p\rangle^{\beta}$ can be considered as a constant within $\mathscr{V}$ was taken into account. The effective coefficients $\langle\mathbf{D}\rangle$ and $\langle\mathbf{m}_0\rangle$ are determined by solving the closure problems detailed in the following section. Comments about the physics of the upscaled model and its coefficients are also provided below, together with some remarks on the existing related literature.

3.2. *Closure problems and macroscopic model*

Substitution of the formal solution given in equations (3.10) into the initial boundary value problem in equations (3.8) and separating the contributions from the two sources, while maintaining the convolution product with the volume source, leads to the following equations for $\mathbf{D}$ and $\mathbf{d}$

$$\int_{t_0=0}^{t_0=t} \left(\nabla \cdot \left.\frac{\partial\mathbf{D}}{\partial t}\right|_{t-t_0}\right) \cdot \left(-\nabla\langle p\rangle^{\beta} + \rho\mathbf{b}\right)_{t_0} dt_0 = \mathbf{0}, \quad \text{in } \mathscr{V}_{\beta},\ t > 0 \tag{3.13a}$$

$$\int_{t_0=0}^{t_0=t}\left[\frac{\rho}{\mu}\left(\left.\frac{\partial^2\mathbf{D}}{\partial t^2}\right|_{t-t_0}+\mathbf{v}_\Delta\cdot\left.\frac{\partial\nabla\mathbf{D}}{\partial t}\right|_{t-t_0}\right)+\left.\frac{\partial\nabla\mathbf{d}}{\partial t}\right|_{t-t_0}-\left.\frac{\partial\nabla^2\mathbf{D}}{\partial t}\right|_{t-t_0}-\mathbf{I}\left.\frac{d\mathscr{H}}{dt}\right|_{t-t_0}\right]\cdot\left(-\nabla\langle p\rangle^\beta+\rho\mathbf{b}\right)_{t_0}dt_0=\mathbf{0},\quad\text{in}\quad\mathscr{V}_\beta,\ t\geqslant 0 \tag{3.13b}$$

$$\int_{t_0=0}^{t_0=t}\left.\frac{\partial\mathbf{D}}{\partial t}\right|_{t-t_0}\cdot\left(-\nabla\langle p\rangle^\beta+\rho\mathbf{b}\right)_{t_0}dt_0=\mathbf{0},\quad\text{at}\quad\mathscr{A}_{\beta\sigma},\ t\geqslant 0 \tag{3.13c}$$

where $\mathscr{H}$ represents the Heaviside function. These equations are completed with periodic boundary conditions for $\mathbf{D}$ and $\mathbf{d}$ and $\langle\partial\mathbf{d}/\partial t\rangle^\beta=\mathbf{0}$. Notice that, at this point, the initial condition for the closure variables has not yet been defined.

In order to satisfy the above equations, valid for any macroscopic forcing $\left(-\nabla\langle p\rangle^\beta+\rho\mathbf{b}\right)$ and at any time, $\mathbf{D}$ and $\mathbf{d}$ must satisfy the following equations, in general (this may be inferred from considering the particular case in which the macroscopic forcing is a constant)

$$\nabla\cdot\frac{\partial\mathbf{D}}{\partial t}=\mathbf{0},\quad\text{in}\quad\mathscr{V}_\beta,\ t>0 \tag{3.14a}$$

$$\frac{\rho}{\mu}\left(\left.\frac{\partial^2\mathbf{D}}{\partial t^2}\right|_\tau+\mathbf{v}\cdot\left.\frac{\partial\nabla\mathbf{D}}{\partial t}\right|_\tau\right)+\left.\frac{\partial\nabla\mathbf{d}}{\partial t}\right|_\tau-\left.\frac{\partial\nabla^2\mathbf{D}}{\partial t}\right|_\tau-\mathbf{I}\left.\frac{d\mathscr{H}}{dt}\right|_\tau=\mathbf{0},\quad\text{in}\quad\mathscr{V}_\beta,\ 0\leqslant\tau\leqslant t;t>0 \tag{3.14b}$$

$$\frac{\partial\mathbf{D}}{\partial t}=\mathbf{0},\quad\text{at}\quad\mathscr{A}_{\beta\sigma},t>0 \tag{3.14c}$$

with τ denoting the elapsed time involved in the convolution product. Note that equation (3.14*b*) is the result of taking the limit $\Delta t\to 0$, so that $\mathbf{v}_\Delta\to\mathbf{v}$. The value of the time step Δ and the information from the rest of the terms in the Taylor expansion in time is hence no longer required.

A subsequent time integration step of equations (3.14) from $\tau=0$ to $\tau=t$ yields

$$\left[\nabla\cdot\mathbf{D}\right]_{\tau=0}^{\tau=t}=\mathbf{0},\quad\text{in}\quad\mathscr{V}_\beta,\quad t>0 \tag{3.15a}$$

$$\left[\frac{\rho}{\mu}\left(\left.\frac{\partial\mathbf{D}}{\partial t}\right|_\tau+\mathbf{v}\cdot\nabla\left.\mathbf{D}\right|_\tau\right)+\nabla\left.\mathbf{d}\right|_\tau-\nabla^2\left.\mathbf{D}\right|_\tau-\mathbf{I}\left.\mathscr{H}\right|_\tau\right]_{\tau=0}^{\tau=t}=\mathbf{0},\quad\text{in}\quad\mathscr{V}_\beta,\quad t>0 \tag{3.15b}$$

$$\left[\mathbf{D}\right]_{\tau=0}^{\tau=t}=\mathbf{0},\quad\text{at}\quad\mathscr{A}_{\beta\sigma},t>0 \tag{3.15c}$$

At this point, initial conditions for $\mathbf{D}$ and $\mathbf{d}$ are chosen to be zero.

As a consequence, equations (3.15) give rise to the following initial and boundary-value problem for the closure variables $\mathbf{D}$ and $\mathbf{d}$

Problem I

$$\nabla \cdot \mathbf{D} = \mathbf{0}, \quad \text{in } \mathscr{V}_\beta,\ t > 0 \tag{3.16a}$$

$$\frac{\rho}{\mu}\left(\frac{\partial \mathbf{D}}{\partial t} + \mathbf{v}\cdot\nabla\mathbf{D}\right) = -\nabla\mathbf{d} + \nabla^2\mathbf{D} + \mathbf{I}, \quad \text{in } \mathscr{V}_\beta,\ t > 0 \tag{3.16b}$$

$$\mathbf{D} = \mathbf{0}, \quad \text{at } \mathscr{A}_{\beta\sigma},\ t > 0 \tag{3.16c}$$

$$\mathbf{D} = \mathbf{0}, \quad \text{when } t = 0 \tag{3.16d}$$

$$\langle \mathbf{d} \rangle^\beta = \mathbf{0}, \quad t > 0 \tag{3.16e}$$

$$\mathbf{D}(\mathbf{r} + \mathbf{l}_i) = \mathbf{D}(\mathbf{r}); \qquad \mathbf{d}(\mathbf{r} + \mathbf{l}_i) = \mathbf{d}(\mathbf{r}), \quad t > 0, \quad i = 1, 2, 3 \tag{3.16f}$$

Note that in equation (3.14*b*), $\mathbf{D}$, $\mathbf{d}$ and $\mathbf{v}$ are all evaluated at the same time t, which improves the exactness of the solution. Practically, this is possible because the pore-scale flow problem in equations (3.8) (the solution of which provides the field of $\mathbf{v}$ at time t) can be solved independently from the closure problem on $\mathbf{D}$ and $\mathbf{d}$. On the basis of this closure problem, it is readily deduced that the contribution from the remaining source (*i.e.*, the initial velocity) leads to the following problem for $\mathbf{m}_0$ and n_0

Problem II

$$\nabla \cdot \mathbf{m}_0 = 0, \quad \text{in } \mathscr{V}_\beta,\ t > 0 \tag{3.17a}$$

$$\frac{\rho}{\mu}\left(\frac{\partial \mathbf{m}_0}{\partial t} + \mathbf{v}\cdot\nabla\mathbf{m}_0\right) = -\nabla n_0 + \nabla^2\mathbf{m}_0, \quad \text{in } \mathscr{V}_\beta,\ t > 0 \tag{3.17b}$$

$$\mathbf{m}_0 = \mathbf{0}, \quad \text{at } \mathscr{A}_{\beta\sigma},\ t > 0 \tag{3.17c}$$

$$\mathbf{m}_0 = \mu\mathbf{v}_0, \quad \text{when } t = 0 \tag{3.17d}$$

$$\langle n_0 \rangle^\beta = 0, \quad t > 0 \tag{3.17e}$$

$$\mathbf{m}_0(\mathbf{r} + \mathbf{l}_i) = \mathbf{m}_0(\mathbf{r}); \qquad n_0(\mathbf{r} + \mathbf{l}_i) = n_0(\mathbf{r}), \quad t > 0, \quad i = 1, 2, 3 \tag{3.17f}$$

As expected, closure problems *I* and *II* are not intrinsic as they depend on the fluid properties and flow conditions or, as will be shown in section 3.4 below, on the Reynolds number characteristic of the flow. A possible way of resolving this issue is to follow an approach used in the homogenization theory, to the cost, however, of making *a priori* scaling assumptions on the viscosity and velocity so that the pore-scale Reynolds number can be expressed as a power of the scale ratio ℓ_β/L (see Sanchez-Palencia (1980), chapter 7, section 4, p.142 and following). This was further investigated by Bourgeat *et al.* (1996) and also by Marušić-Paloka & Mikelić (2000) in the steady regime, but the procedure could be carried out for a power on the Reynolds number up to 0 (see also (Balhoff *et al.* 2010)). The approach followed here is quite different and leads to closure problems that depend on the pore-scale flow field, or more precisely, on the macroscopic forcing, as will be shown below. Indeed, an alternative formulation of the closure problems *I* and *II* is possible by substituting the formal solution given in equation (3.10*a*) into the convective terms of the closure problems to obtain

$$\frac{\rho}{\mu}\left[\frac{\partial \mathbf{D}}{\partial t} + \frac{1}{\mu}\left(\frac{\partial \mathbf{D}}{\partial t} * \cdot\left(-\nabla\langle p\rangle^\beta + \rho\mathbf{b}\right) + \mathbf{m}_0\right)\cdot\nabla\mathbf{D}\right] = -\nabla\mathbf{d} + \nabla^2\mathbf{D} + \mathbf{I}, \quad \text{in } \mathscr{V}_\beta,\ t > 0 \tag{3.18a}$$

$$\frac{\rho}{\mu}\left[\frac{\partial \mathbf{m}_0}{\partial t} + \frac{1}{\mu}\left(\frac{\partial \mathbf{D}}{\partial t} * \cdot\left(-\nabla\langle p\rangle^\beta + \rho\mathbf{b}\right) + \mathbf{m}_0\right)\cdot\nabla\mathbf{m}_0\right] = -\nabla n_0 + \nabla^2\mathbf{m}_0, \quad \text{in } \mathscr{V}_\beta,\ t > 0 \tag{3.18b}$$

These equations are interesting from a fundamental viewpoint because they show that

the closure problems are ultimately not functions of the velocity but of the macroscopic forcing given by $-\nabla\langle p\rangle^{\beta}+\rho\mathbf{b}$ and the initial field of the velocity, $\mathbf{v}_0$. However, from a practical viewpoint this formulation is not attractive because it involves the coupled and non-local in time solution of both closure problems, which have also become nonlinear. For the sake of ease in the computations, the strategy to follow is: 1) solve the flow problem given by equations (3.8) and 2) substitute the solution of the velocity into closure problems *I* and *II* written in the form given in equations (3.16) and (3.17), which is linear because the numerical solution of $\mathbf{v}$ does not require knowledge of the closure variables. Note that, in both approaches, the inputs are the macroscopic driving force and the initial flow condition. The dependence on the latter is lost under steady flow and both functionalities are not present under creeping flow conditions. In fact, only in this very specific case, the closure problems are intrinsic.

Letting

$$\mathbf{H}_t=\langle\mathbf{D}\rangle \tag{3.19a}$$

$$\boldsymbol{\alpha}=\frac{\langle\mathbf{m}_0\rangle}{\mu} \tag{3.19b}$$

the macroscopic momentum equation (3.12*b*) can be finally written as

$$\langle\mathbf{v}\rangle=-\frac{1}{\mu}\frac{\partial\mathbf{H}_t}{\partial t}*\cdot\left(\nabla\langle p\rangle^{\beta}-\rho\mathbf{b}\right)+\boldsymbol{\alpha},\quad\text{in }\mathscr{V}_{Mh},\ t>0 \tag{3.20}$$

or, equivalently

$$\langle\mathbf{v}\rangle=-\frac{1}{\mu}\frac{\partial}{\partial t}\left(\mathbf{H}_t*\cdot\left(\nabla\langle p\rangle^{\beta}-\rho\mathbf{b}\right)\right)+\boldsymbol{\alpha},\quad\text{in }\mathscr{V}_{Mh},\ t>0 \tag{3.21}$$

and this represents one of the major results of this work. It clearly shows the existence of a memory effect expressed by the convolution product that was anticipated by Auriault (1980) leading to an unsteady macroscopic momentum equation, which does not resemble the heuristic model given by

$$\rho\frac{\partial\langle\mathbf{v}\rangle^{\beta}}{\partial t}=-\left(\nabla\langle p\rangle^{\beta}-\rho\mathbf{b}\right)-\mu\varepsilon\mathbf{H}^{-1}\cdot\langle\mathbf{v}\rangle^{\beta},\quad\text{in }\mathscr{V}_{Mh},\ t>0 \tag{3.22}$$

where $\mathbf{H}$ is the steady *apparent permeability* tensor introduced by Whitaker (1996) for the average model of steady inertial one-phase flow in homogeneous porous media. The two models only match under steady conditions. This can be proved, for instance, by considering that the macroscoping forcing remains constant after a given time. Under such conditions, $\boldsymbol{\alpha}\to\mathbf{0}$ in the long time limit. Moreover, in this time limit, closure problem *I* in equations (3.16) conveniently coincides with the one obtained by Whitaker (1996) for steady inertial flow in homogeneous porous media and $\mathbf{H}_t\to\mathbf{H}$. Under these circumstances, the final value theorem applied to equations (3.20) (or (3.21)) indicates that the average model derived above reduces to the steady form of the macroscopic inertial momentum equation (3.22) also reported by Whitaker (1996).

In the macroscopic equation (3.20) (or (3.21)), $\mathbf{H}_t$ is homogeneous to a permeability and shall be referred to as the *dynamic apparent permeability* tensor, the apparent character being inherent to its dependence on inertial effects. It should be noticed that, except in the creeping flow regime, the effective coefficient $\mathbf{H}_t$ depends on the initial condition and on the macroscopic forcing through the convective inertial term in closure problem *I*. In addition, $\boldsymbol{\alpha}$, which has the unit of a velocity, only contains a source due to the initial velocity field, $\mathbf{v}_0$, and is zero when $\mathbf{v}_0=\mathbf{0}$. However, the values of $\boldsymbol{\alpha}$ are also driven by the macroscopic forcing by means of the convective term in problem *II*. It is

important to emphasize this feature and make clear that the effective coefficients are not functions of the average velocity, which would result in a misleading macroscale model given in equation (3.20). Unfortunately, the dependence of the coefficients on the macroscopic forcing and the initial condition is not trivial and, as a consequence, an explicit functionality of the seepage velocity with them is not easily achievable, in general. Under non-inertial conditions, the dependence of the macroscale velocity on the macroscopic forcing is linear, albeit the dependence on the initial flow is still not trivial. For steady, creeping flow, the well-known linear dependence of the velocity on the macroscopic forcing is recovered in the form of Darcy's law.

The model reported in equation (3.20) generalizes to inertial flow the result reported by Allaire (1992) for the creeping regime, which was also studied by Lions (1981) and later by Mikelić (1994). When restricted to this particular type of flow, the macroscale momentum equation (3.20) matches that reported in the two latter references only when the initial flow is zero. The discrepancy observed when $\mathbf{v}_0 \neq \mathbf{0}$ lies in the fact that, as mentioned above (section 3.1), a particular form of the initial condition was considered by Lions (1981) and Mikelić (1994) for the problem in the periodic unit cell. This special form of the boundary condition was however not retained by Allaire (1992) nor in the present work. In the particular case of creeping flow and $\mathbf{v}_0 = \mathbf{0}$, envisaged by Mei & Vernescu (2010), agreement is also found with the result of this reference. In Mikelić (1994), both creeping and inertial flows were considered; unfortunately, no local closure problem was derived for the inertial case. In the work by Allaire (1992), $\mathbf{A}$ identifies with $\frac{\partial \mathbf{K}_t}{\partial t}$ and $\mathbf{a}$ with $\boldsymbol{\alpha}$, $\mathbf{K}_t$ being the *dynamic permeability* equivalent to $\mathbf{H}_t$ under non-inertial flow conditions. It must be emphasized that $\mathbf{A}$ should not be called "*permeability*" as it is dimensionally incorrect. This terminology is also improperly used in the works by Mikelić (1994) and Mei & Vernescu (2010). Without inertia and when $\mathbf{v}_0 = \mathbf{0}$, the average model derived above also corresponds to the one presented by Auriault *et al.* (1985), Sheng & Zhou (1988) or Zhou & Sheng (1989) (see also (Sahimi 2011)) and considered by Johnson *et al.* (1987) that was obtained in the Fourier space.

Regarding the ancillary closure problems related to the macroscopic models mentioned above, closure problems *I* and *II*, under creeping flow conditions, coincide with those reported by Allaire (1992). However, under these conditions, closure problem *I* does not correspond to the ancillary problems reported by Mikelić (1994) and by Mei & Vernescu (2010). The closure problems in these two references lack of compatibility between the initial and boundary conditions, thus leading to a non-regular solution as admitted by Mikelić (1994). This discrepancy is only technical and can be solved by an appropriate change of variables in the Laplace domain, leading to a modification of the initial condition, compatible with the interfacial boundary condition. Consistently, in the creeping regime, the Laplace-transformed version of closure problem *I* is also identical to that given by Sheng & Zhou (1988), Zhou & Sheng (1989), Mikelić (1994) and Mei & Vernescu (2010) for their corresponding so-called "*permeability*".

It shall be noticed that in a paper by Lions & Masmoudi (2005), an attempt to use the homogenization method to upscale the unsteady Navier-Stokes equations was presented. Unfortunately, the authors only succeeded to use the two-scale convergence method for the case of perfect flow (*i.e.*, the unsteady Euler equation) and attributed their failure to upscale the unsteady incompressible Navier-Stokes equations to the existence of boundary layers. In fact, in their study no upscaled model or closure problems were provided. The drawback arising from boundary layers was also mentioned by Masmoudi (1998) and was later circumvented by the same author for the case of compressible flow (see Masmoudi (2002)). Nevertheless, the development in this later reference yields a semi-stationary macroscopic model. The difficulty encountered by these authors arises from the fact that

the solution is sought in a weak sense. It is not present in the approach followed in the current analysis.

Further considering the very particular case of the creeping regime for which the initial flow condition is such that $\mathbf{v}_0$ obeys a Stokes model, it can be proved that the macroscopic model derived above can be formulated in such a way that closure problem I is the only one that needs to be solved. The proof is provided in Appendix A.

Before illustrating the solution of closure problems I and II with some numerical results, it is of interest to analyse the symmetry and positiveness properties of $\mathbf{H}_t$ and this is the object of the next section.

3.3. *Symmetry properties and positiveness of* $\boldsymbol{H}_t$

The symmetry analysis of $\mathbf{H}_t$ is carried out following the approach developed in Lasseux & Valdés-Parada (2017) and the reader is referred to this article for details of the derivations, in particular section II A therein. It must be noticed that no special assumption is needed on the pore-structure within the periodic unit cell representative of the material on which closure problem I is to be solved.

The analysis starts by redirecting the attention to equation (3.14*b*), which is considered at any value of $0 \leqslant \tau \leqslant t$ for a given value of t. Pre-multiplication by $\left.\dfrac{\partial \mathbf{D}^T}{\partial t}\right|_{t-\tau}$, together with a subsequent time-integration from $\tau = 0$ to $\tau = t$ and the application of the superficial averaging operator leads to

$$\frac{\rho}{\mu}\frac{\partial}{\partial t}\langle \mathbf{M}^T * \cdot \mathbf{M}\rangle + \frac{\rho}{\mu}\langle \mathbf{M}^T * \cdot \mathbf{v}\cdot\nabla\mathbf{M}\rangle = \\ -\langle \mathbf{M}^T * \cdot \nabla\mathbf{m}\rangle + \langle \mathbf{M}^T * \cdot \nabla^2\mathbf{M}\rangle + \frac{d\mathbf{H}_t^T}{dt}, \quad t > 0 \tag{3.23}$$

where, for simplicity in notation, $\mathbf{M} = \partial\mathbf{D}/\partial t$ and $\mathbf{m} = \partial\mathbf{d}/\partial t$. Notice that $\mathbf{M} = \mathbf{0}$ at $t = 0$, in accordance with equation (3.16*b*), given the initial condition for $\mathbf{D}$.

The first term on the left hand side of equation (3.23) is clearly symmetric. As shown in Lasseux & Valdés-Parada (2017), the first term on the right hand side is zero using the solenoidal character of $\mathbf{M}$, the no-slip boundary condition, periodicity and the averaging theorem. On the same basis, it can also be proved that $\left\langle \mathbf{M}^T * \cdot \nabla^2\mathbf{M}\right\rangle = -\left\langle (\nabla\mathbf{M})^{T3} * : \nabla\mathbf{M}\right\rangle$ where the superscript $T3$ stands for the transpose that permutes the first and third indices of a third-order tensor and : is the double dot product in the sense of the nested convention. This last term can be shown to be symmetric. Finally, the second term on the left hand side of equation (3.23) is skew-symmetric. The proof of this can be carried out on the basis of equations (12) and (13) in section II.A in the work by Lasseux & Valdés-Parada (2017), when extended to the case where a convolution product is involved.

From the above, the time rate of change of the dynamic apparent permeability tensor can hence be expressed as follows

$$\frac{\partial \mathbf{H}_t}{\partial t} = \underbrace{\frac{\rho}{\mu}\frac{\partial}{\partial t}\left\langle \frac{\partial \mathbf{D}^T}{\partial t} *\cdot \frac{\partial \mathbf{D}}{\partial t}\right\rangle + \left\langle \left(\nabla \frac{\partial \mathbf{D}}{\partial t}\right)^{T3} *: \left(\nabla \frac{\partial \mathbf{D}}{\partial t}\right)\right\rangle}_{symmetric\ part}$$
$$\underbrace{-\frac{\rho}{\mu}\left\langle \frac{\partial \mathbf{D}^T}{\partial t} *\cdot \left(\nabla \cdot \left(\mathbf{v}\frac{\partial \mathbf{D}}{\partial t}\right)\right)\right\rangle}_{skew-symmetric\ part}, \quad t > 0 \tag{3.24}$$

which provides the decomposition of $\mathbf{H}_t$ into its irreducible parts because the operation of time integration does not alter the symmetry properties of a tensor. It should be noticed that the skew-symmetric part is only due to the existence of inertial transport, thus extending the result given in section II.A of the work by Lasseux & Valdés-Parada (2017) to unsteady conditions. As a corollary, it can be concluded that in the creeping regime, $\mathbf{K}_t$ is a symmetric tensor at all times (and therefore the intrinsic permeability is also a symmetric tensor).

At this point, the focus should be laid upon the positiveness property of $\mathbf{H}_t$ and, for convenience, the analysis is carried out in the Laplace domain. A starting point of the derivation is the following identity, which holds for any constant but arbitrary vector $\boldsymbol{\lambda}$

$$\boldsymbol{\lambda} \cdot \overline{\mathbf{H}}_t \cdot \boldsymbol{\lambda} = \boldsymbol{\lambda} \cdot \overline{\mathbf{H}}_t^T \cdot \boldsymbol{\lambda} \tag{3.25}$$

where overlined variables denote the Laplace transform of their temporal counterparts. This implies that

$$\boldsymbol{\lambda} \cdot \left(\overline{\mathbf{H}}_t + \overline{\mathbf{H}}_t^T\right) \cdot \boldsymbol{\lambda} = 2\boldsymbol{\lambda} \cdot \overline{\mathbf{H}}_t \cdot \boldsymbol{\lambda} \tag{3.26}$$

Applying the Laplace transform to equation (3.24), adding the result to its transpose and pre- and post- multiplying the ensuing expression by $\boldsymbol{\lambda}$ while making use of equation (3.26), yields

$$\boldsymbol{\lambda} \cdot \overline{\mathbf{H}}_t \cdot \boldsymbol{\lambda} = \frac{\rho}{\mu} s^2 \langle \boldsymbol{\lambda} \cdot \overline{\mathbf{D}}^T \cdot \overline{\mathbf{D}} \cdot \boldsymbol{\lambda} \rangle + s \langle \boldsymbol{\lambda} \cdot \left(\nabla \overline{\mathbf{D}}\right)^{T3} : \nabla \overline{\mathbf{D}} \cdot \boldsymbol{\lambda} \rangle \tag{3.27}$$

Here s denotes the symbolic Laplace variable. The first term on the right-hand side of this expression can be written as

$$\langle \boldsymbol{\lambda} \cdot \overline{\mathbf{D}}^T \cdot \overline{\mathbf{D}} \cdot \boldsymbol{\lambda} \rangle = \langle \left(\overline{\mathbf{D}} \cdot \boldsymbol{\lambda}\right) \cdot \left(\overline{\mathbf{D}} \cdot \boldsymbol{\lambda}\right) \rangle = \langle \left(\overline{\mathbf{D}} \cdot \boldsymbol{\lambda}\right)^2 \rangle \tag{3.28}$$

which is a positive definite quantity. Turning the attention to the second average term on the right-hand side of equation (3.27) and making use of the Gibbs and Einstein notations, one can write

$$\begin{aligned} \langle \boldsymbol{\lambda} \cdot \left(\nabla \overline{\mathbf{D}}\right)^{T3} : \nabla \overline{\mathbf{D}} \cdot \boldsymbol{\lambda} \rangle &= \langle \lambda_k \left(\nabla \overline{\mathbf{D}}\right)^{T3}_{kij} \left(\nabla \overline{\mathbf{D}}\right)_{jil} \lambda_l \rangle \\ &= \langle \lambda_k \left(\nabla \overline{\mathbf{D}}\right)_{jik} \left(\nabla \overline{\mathbf{D}}\right)_{jil} \lambda_l \rangle \\ &= \left\langle \left(\left(\nabla \overline{\mathbf{D}}\right)_{jik} \lambda_k\right)^2 \right\rangle \end{aligned} \tag{3.29}$$

which proves that this term is also definite positive. Since s is positive, it can be concluded that $\overline{\mathbf{H}}_t$ is a positive definite tensor. A corollary of the above is that $\overline{\mathbf{K}}_t$ is a symmetric definite positive tensor that hence admits an inverse. However, the proof provided here does not allow to conclude that the same applies to $\overline{\mathbf{H}}_t$.

3.4. *Closure problem solution*

From the above derivations, it follows that closure problems *I* and *II* can be solved using standard unsteady Navier-Stokes solvers. The mathematical structure of these problems indicates that closure variable $\mathbf{D}$ is a time-increasing field because the initial condition is homogeneous and the source term in the momentum-like equation is a positive constant. Consequently, the effective coefficient $\mathbf{H}_t$ should be expected to exhibit similar dynamics. On the contrary, in *Problem II*, the only source is the initial condition and therefore both the $\mathbf{m}_0$ field and coefficient $\boldsymbol{\alpha}$ can be expected to be time-decaying.

Before proceeding to the validation of the average model, it is convenient to direct the attention to the solution of the local closure problems *I* and *II* so that the dynamics of the effective coefficients can be examined. To this end, it is worth expressing the closure problems and the effective coefficients in the following dimensionless form:

Problem I*

$$\nabla^* \cdot \mathbf{D}^* = \mathbf{0}, \quad \text{in } \mathscr{V}_\beta,\ t^* > 0 \tag{3.30a}$$

$$\frac{\partial \mathbf{D}^*}{\partial t^*} + Re\mathbf{v}^* \cdot \nabla^* \mathbf{D}^* = -\nabla^* \mathbf{d}^* + \nabla^{*2}\mathbf{D}^* + \mathbf{I}, \quad \text{in } \mathscr{V}_\beta,\ t^* > 0 \tag{3.30b}$$

$$\mathbf{D}^* = \mathbf{0}, \quad \text{at } \mathscr{A}_{\beta\sigma},\ t^* > 0 \tag{3.30c}$$

$$\mathbf{D}^* = \mathbf{0}, \quad \text{when } t^* = 0 \tag{3.30d}$$

$$\langle \mathbf{d}^* \rangle^\beta = \mathbf{0}, \quad t^* > 0 \tag{3.30e}$$

$$\mathbf{D}^*(\mathbf{r}^* + \mathbf{l}_i^*) = \mathbf{D}^*(\mathbf{r}^*); \qquad \mathbf{d}^*(\mathbf{r}^* + \mathbf{l}_i^*) = \mathbf{d}^*(\mathbf{r}^*), \quad t^* > 0, \quad i = 1, 2, 3 \tag{3.30f}$$

where the dimensionless version of the dynamic apparent permeability tensor is obtained from

$$\mathbf{H}_t^* = \langle \mathbf{D}^* \rangle \tag{3.31}$$

Problem II*

$$\nabla^* \cdot \mathbf{m}_0^* = 0, \quad \text{in } \mathscr{V}_\beta,\ t^* > 0 \tag{3.32a}$$

$$\frac{\partial \mathbf{m}_0^*}{\partial t^*} + Re\mathbf{v}^* \cdot \nabla^* \mathbf{m}_0^* = -\nabla n_0^* + \nabla^{*2}\mathbf{m}_0^*, \quad \text{in } \mathscr{V}_\beta,\ t^* > 0 \tag{3.32b}$$

$$\mathbf{m}_0^* = \mathbf{0}, \quad \text{at } \mathscr{A}_{\beta\sigma},\ t^* > 0 \tag{3.32c}$$

$$\mathbf{m}_0^* = \mathbf{v}_0^*, \quad \text{when } t^* = 0 \tag{3.32d}$$

$$\langle n_0^* \rangle^\beta = 0, \quad t^* > 0 \tag{3.32e}$$

$$\mathbf{m}_0^*(\mathbf{r}^* + \mathbf{l}_i^*) = \mathbf{m}_0^*(\mathbf{r}^*); \qquad n_0^*(\mathbf{r}^* + \mathbf{l}_i^*) = n_0(\mathbf{r}^*), \quad t^* > 0, \quad i = 1, 2, 3 \tag{3.32f}$$

The solution of this problem can be used to obtain

$$\boldsymbol{\alpha}^* = \langle \mathbf{m}_0^* \rangle \tag{3.33}$$

The above problems are written in terms of the following definitions:

$$\begin{gathered} t^* = \frac{\mu t}{\rho \ell^2}; \quad \mathbf{x}^* = \frac{\mathbf{x}}{\ell}; \quad \mathbf{v}^* = \frac{\mathbf{v}}{v_{ref}}; \quad \mathbf{D}^* = \frac{\mathbf{D}}{\ell^2}; \quad \mathbf{d}^* = \frac{\mathbf{d}}{\ell}; \quad \mathbf{H}_t^* = \frac{\mathbf{H}_t}{\ell^2} \\ \mathbf{m}_0^* = \frac{\mathbf{m}_0}{\mu v_{ref}}; \quad n_0^* = \frac{n_0 \ell}{\mu v_{ref}}; \quad \boldsymbol{\alpha}^* = \frac{\boldsymbol{\alpha}}{v_{ref}}; \quad Re = \frac{\rho v_{ref} \ell}{\mu} \end{gathered} \tag{3.34}$$

where ℓ is the size of the geometrical periodic unit cell (see figure 2). As expected, the closure problems are dependent on $\mathbf{v}^*$. Consequently, the values of the effective coefficients

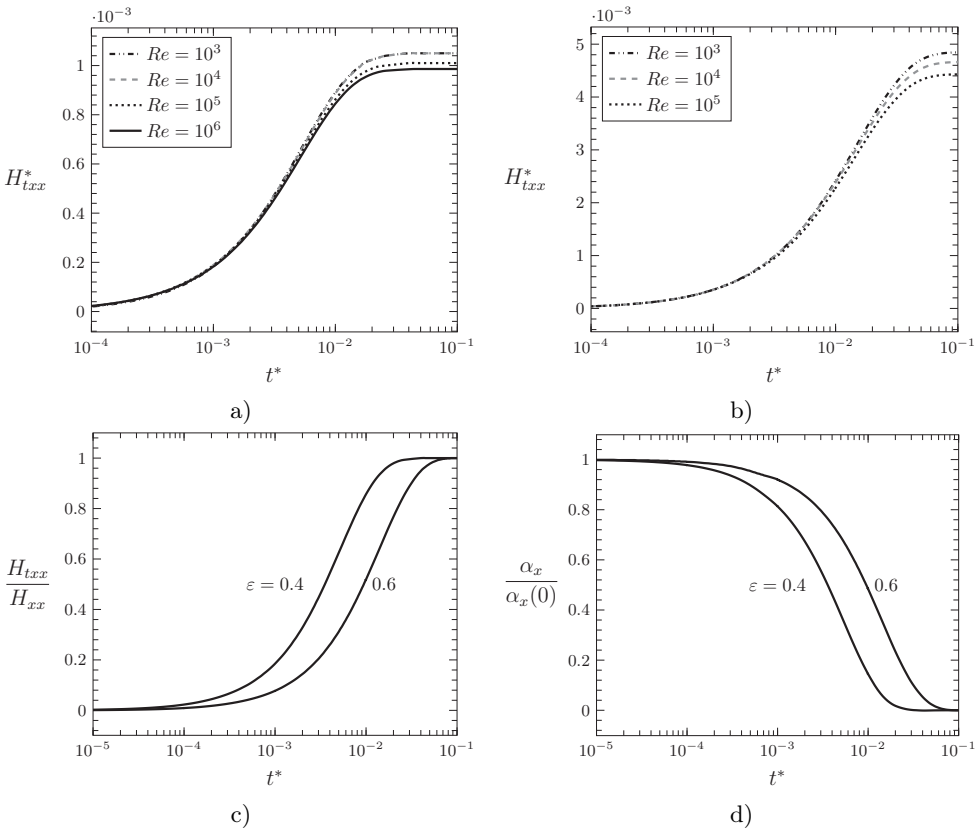

FIGURE 3. Dynamics of the xx component of the apparent permeability tensor (a-c) and of the x-component of vector $\boldsymbol{\alpha}$ (d) for the flow problem described in section 4.1. The predictions result from solving the closure problems I and II in the unit cell depicted in figure 2 taking: a) $\varepsilon = 0.4$, b) $\varepsilon = 0.6$. In c) results are presented after normalization with the steady value of the apparent permeability and in d) results are normalized with the initial value of α_x.

are sensitive to the different flow conditions considered in the pore-scale model. Here and in the rest of this work, it is assumed that the macroscopic driving force is in the horizontal x-axis direction. In the following section, several case studies are considered for validation with DNS, of which, the predictions of the effective coefficients corresponding only to *Case I* (see section 4.1) are shown here for the purpose of illustration. All the simulations presented in this work were performed using the commercial finite element software Comsol Multiphysics 5.2. The direct MUMPS solver included in the program was used and standard (spatial and temporal) meshing convergence analyses were carried out in order to ensure that results are independent of these numerical degrees of freedom. In accordance with the case study of section 4.1, the dimensionless macroscopic pressure gradient experiences a step change at $t^* = 0$ from 0.1 to 1.0 as expressed in equation (4.5), while Re, ranging from 10^3 up to 10^6, is maintained the same before and after the change of the macroscopic pressure gradient.

In figure 3, predictions of the dimensionless xx-component of $\mathbf{H}_t$ (*i.e.*, H^*_{txx}) and of the x-component of $\boldsymbol{\alpha}$ (*i.e.*, α_x), resulting from the closure problem solution in the unit cell depicted in figure 2, are reported for two porosity values ($\varepsilon = 0.4$ and 0.6). Values of the Reynolds number were kept smaller than the critical one characteristic of the first Hopf bifurcation which, for the structure under consideration, is identified to be $\sim 10^6$ for $\varepsilon =$

0.4 and $\sim 10^5$ for $\varepsilon = 0.6$ (see figure 10 in Agnaou *et al.* 2016). Consequently, the solution remains time-independent after steady-state is reached. Results on H^*_{txx}, shown in figures 3a) and b), indicate that the influence of inertial transport is not only experienced at early times (*i.e.*, $t^* < 10^{-4}$), but during intermediate times (*i.e.*, $t^* > 10^{-3}$) and until steady state is reached (*i.e.*, $H_{txx} \to H_{xx}$). By comparing the dynamics of the apparent permeability shown in these two graphs, it is clear that porosity plays quite a significant role since the time at which H_{txx} reaches H_{xx}, for $\varepsilon = 0.6$, is significantly larger than the one for $\varepsilon = 0.4$. In this last case, it is worth noticing that the curves of H_{txx} remain almost unchanged over the whole range of time for $Re \leqslant 10^4$, whereas in figure 3b) the curves for $Re = 10^3$ and $Re = 10^4$ can be clearly differentiated. These observations are consistent with those reported by Lasseux *et al.* (2011) under steady conditions.

The shape of the curves shown in figures 3a) and b) suggests a subsequent normalization by the steady state value, H_{xx}, of H_{txx}, so that the dependence on the Reynolds number is no longer present. This is indeed the case as reported in figure 3c), which follows from the ideas proposed by Sheng & Zhou (1988). The normalized dynamic apparent permeability may then be represented by a linear combination of exponential linear functions of times. The same type of normalization can be applied to α^*_x, but in this case with respect to the initial value since it is the maximum one. Results are presented in figure 3d) showing that this normalization yields a master curve for the dynamics of $\boldsymbol{\alpha}$ for Reynolds numbers as high as 10^6. The dynamics of $\boldsymbol{\alpha}$ exhibits a temporal dependence, which can be represented by a Boltzmann-type function. This contrasts with the purely exponential decay suggested by Mikelić (1994) for periodic structures.

The master curves for the effective coefficients are distinct for different porosities, and for the simple geometry considered here, it appears that the steady state is reached faster as the solid phase occupies a larger fraction of the unit cell, which was also the case for H_{txx}. These results evidence that the effective coefficients are bound functions of time and are sensitive to the topology of the unit cell and to the flow conditions, in general.

4. Results

At this point of the analysis, it is pertinent to compare predictions resulting from the upscaled model with those from solving the pore-scale model, *i.e.*, from direct numerical simulations (DNS). This comparison is required to validate the macroscale model. To this end, consider as a solution domain of the pore-scale model, an array of n inline unit cells of side length ℓ, each containing a square obstacle to represent the solid phase as sketched in figure 4. For the sake of simplicity and without any loss of generality, body forces are disregarded for the rest of the analysis, so that the pore-scale momentum transport equation can be expressed in a dimensionless form as

$$\frac{\partial \mathbf{v}^*}{\partial t^*} + Re\mathbf{v}^* \cdot \nabla^* \mathbf{v}^* = -\nabla^* p^* + \nabla^{*2}\mathbf{v}^*, \quad \text{in } \mathscr{V}_\beta,\ t > 0 \tag{4.1}$$

where $p^* = p\ell/(\mu v_{ref})$. In order for the pressure gradient to be unitary at the scale of the unit cell, the reference velocity was chosen to be given by $v_{ref} = \ell^2 \|\nabla \langle p \rangle^\beta_s\|/\mu$, $\|\nabla \langle p \rangle^\beta_s\|$ being the maximum value of the pressure gradient over the entire time range of observation of the flow process. In this way, the following boundary conditions can be applied at the edges of the macroscopic domain

$$\text{at } x^* = 0, \quad p^* = nf(t^*), \quad \forall y^*, t^* > 0 \tag{4.2}$$

$$\text{at } x^* = n, \quad p^* = 0, \quad \forall y^*, t^* > 0 \tag{4.3}$$

FIGURE 4. Solution domain for the direct numerical simulations consisting of an array of n inline square unit cells of length ℓ.

with $f(t^*)$ being a known function of time that may be applicable to a single unit cell. In addition, periodic conditions at the horizontal boundaries are applied, *i.e.*

$$\mathbf{v}^*(x^*, 0) = \mathbf{v}^*(x^*, 1), \quad \forall x^*, t^* > 0 \tag{4.4}$$

The dimensionless problem was solved for values of t^* ranging from 10^{-11} up to 10 and, in the rest of this section, results are presented only for a porosity value of 0.4. Similar predictions were obtained for other porosity values. In order to determine the number of unit cells to be considered in the solution domain, so that the results are collected in $\mathscr{V}_{Mh}$ for given flow conditions, a criterion was chosen such that the value of the intrinsic average of the x-component of $\mathbf{v}^*$ located at the $(n+1)/2$ unit cell (with n being an odd number) does not vary by more than $10^{-5}\%$ when n is increased by 2. A value of $n = 21$ was found appropriate to satisfy this criterion and was hence used as the size of the macroscopic domain in the remainder of the present analysis.

Simulations of the upscaled model were performed in the following manner. Firstly, the initial and dimensionless velocity field (say, $\mathbf{v}_0^*$) was determined in a single unit cell from the solution of the steady version of the pore-scale model for a given initial macroscopic pressure gradient (say $\nabla^* \langle p_0^* \rangle^\beta$) and Reynolds number Re. Secondly, the unsteady pore-scale model was solved subject to a desired unsteady macroscopic pressure gradient, keeping Re the same. The information from the solution of these two problems was then used to predict the fields of the closure variables $\mathbf{D}$ and $\mathbf{m}_0$, for the prescribed value of Re, from which the effective-medium coefficients, $\mathbf{H}_t$ and $\boldsymbol{\alpha}$, were computed. Once these coefficients are available at all times, they were substituted into the closed upscaled model in order to predict the dynamics of the macroscopic velocity.

Results are organized in case studies as follows: i) A step change of the pressure gradient from the initial condition to its steady value; ii) A smooth time-decaying flow that leaves the system at rest at steady state; iii) A single pressure gradient pulse and iv) An oscillatory flow.

For completeness of the comparison of the different approaches, it is also pertinent to compare the DNS results with the predictions arising from the heuristic model given in equation (3.22). Notice that this model does not require knowledge of the dynamics of the apparent permeability tensor as it only involves its steady value. For all the case studies, the value of H_{xx}^* in the heuristic model was computed with the value of Re of interest and the unitary dimensionless pressure gradient along the horizontal x-axis (Lasseux *et al.* 2011).

4.1. *Case study I: Step change of the pressure gradient*

The first two case studies deal with the dynamics from one steady state to another, which is a physical situation that can be of interest in control engineering or in measurements of the dynamic apparent permeability, to cite just few examples. The goal is to examine the dynamics of the macroscopic velocity and the role played by the initial flow condition. To this end, let the first case study deal with a step change of the pressure gradient. In

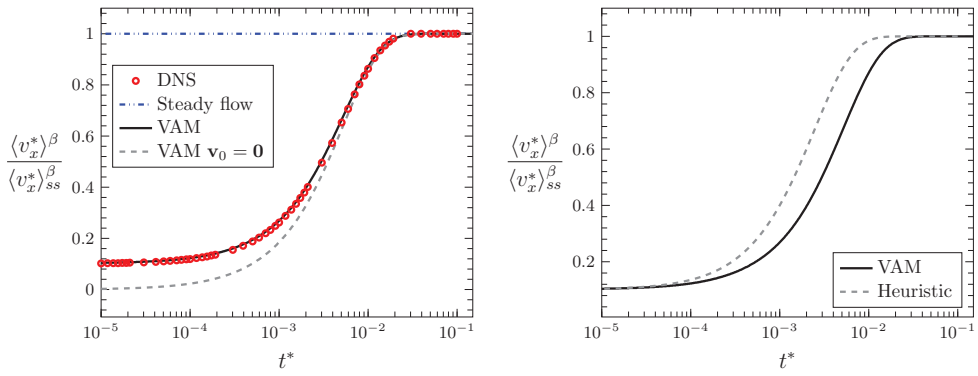

FIGURE 5. Dynamics of the x-component of the macroscale velocity vector, normalized by its steady-state value $\langle v_x^* \rangle^\beta_{ss}$, resulting from the step change on the pressure gradient given in equation (4.5). In a) predictions correspond to direct numerical simulations and from the volume averaging method with and without inclusion of the initial flow. In b) a comparison is shown between predictions from the volume averaging method and the heuristic model. Simulations correspond to a porosity of 0.4 and $Re = 10^6$.

this way, consider the flow at $t^* \leqslant 0$ to be steady resulting from a dimensionless pressure gradient value of 0.1. Then suddenly, at $t^* > 0$, let this gradient become unitary, *i.e.*,

$$-\frac{\partial \langle p^* \rangle^\beta}{\partial x^*} = \begin{cases} 0.1, & t^* \leqslant 0 \\ 1.0, & t^* > 0 \end{cases} \tag{4.5}$$

In figure 5a), the response of the system to this forcing is presented in terms of the predicted evolutions of the macroscale velocity obtained from DNS, together with those from the volume averaging method (VAM). Simulations correspond to $Re = 10^6$ and they match those for $Re = 10^3$ since results are normalized by the final steady-state value of the velocity (*i.e.*, $\langle v_x^* \rangle^\beta_{ss}$). This is consistent with the observations made for H_{txx} presented in the previous section. Clearly, the agreement between DNS and VAM is excellent at all times.

Notice that the steady-state regime is reached at $t^* > 0.03$. In order to have an idea of the time span over which the initial condition is playing a relevant role in the macroscale model, predictions are presented for the case in which $\mathbf{v}_0 = \mathbf{0}$ (*i.e.*, $\nabla^* \langle p_0^* \rangle^\beta = 0$). Under these conditions, closure problem *II* is completely homogeneous and its solution is zero for all $\mathbf{x}$ (*i.e.*, $\boldsymbol{\alpha} = \mathbf{0}$). In this case, it is noticed that the predictions only match those from DNS after $t^* > 0.01$, thus illustrating that the initial condition has a significant effect during almost the entire time range in which $\langle v_x^* \rangle^\beta$ is time-dependent. Finally, in figure 5b), the dynamics of the average velocity resulting from VAM are compared with those obtained from the heuristic model. The latter clearly overpredicts the velocity dynamics in a time range that roughly spans through three orders of magnitude. As expected, both approaches match at times close to the initial condition and at steady state. This is consistent with the fact that both the heuristic and upscaled models depart from the same initial condition and both converge towards the classical Darcy-like model at sufficiently large time.

4.2. *Case study II: Time-decaying pressure gradient*

As a second case study, consider another change of steady state with two major differences from the previous one: first, let the maximum flow be settled at $t^* \leqslant 0$ and second, let

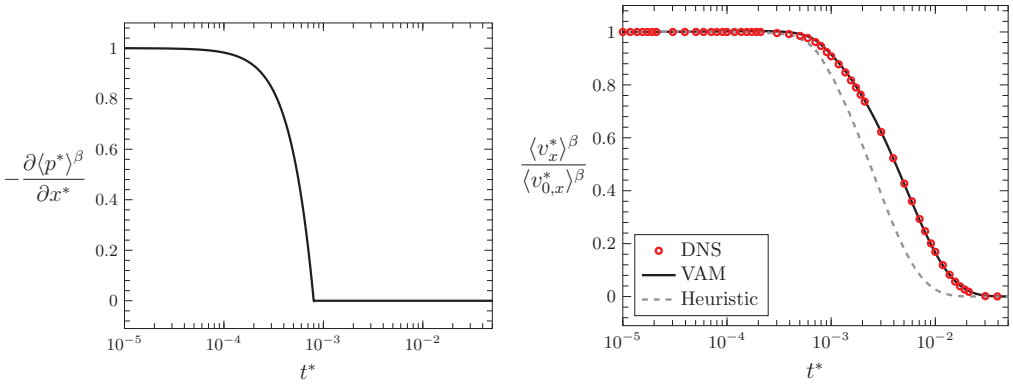

FIGURE 6. a) Dynamics of the decaying macroscopic pressure gradient given in equation (4.6) taking $t_m^* = 8\times10^{-4}$ and $\omega^* = 1000$. b) Dynamics of the x-component of the macroscale velocity vector, normalized by its initial value $\langle v_{0,x}^*\rangle^\beta$, resulting from the time-decaying macroscopic pressure gradient. Predictions result from performing direct numerical simulations, and from the solution of the macroscale model obtained by the volume averaging method and the heuristic model. Simulations correspond to a porosity of 0.4 and $Re = 10^6$.

the macroscopic pressure gradient decay smoothly according to the following expression:

$$-\frac{\partial\langle p^*\rangle^\beta}{\partial x^*} = \begin{cases} 1 - \dfrac{t^*\sin(\omega^* t^*)}{t_m^*\sin\omega^* t_m^*}, & 0 \leqslant t^* \leqslant t_m^* \\ 0, & t^* > t_m^* \end{cases} \tag{4.6}$$

with t_m^* and ω^* representing the dimensionless maximum time at which the pressure gradient is non-zero and a given non-dimensional frequency, respectively. The value of t_m^* was chosen to be smaller than the dimensionless time at which the initial flow was observed to be insensitive in the previous case and was fixed to 8×10^{-4}. In order to avoid oscillations, a value of 1000 was chosen for ω^*, yielding the smooth decaying dynamics of the macroscopic pressure gradient shown in figure 6a). This flow condition may correspond to physical situations in which the pumping device is slowly turned off. Furthermore, for this particular flow condition, $H_{txx}^* \to K_{xx}^*$ at steady state. This is to be expected because both acceleration and convective inertial effects are no longer present at late times.

In figure 6b), the comparison of the predictions of $\langle v_x^*\rangle^\beta$ resulting from DNS with those from the upscaled model derived in this work and from the heuristic model for the flow conditions described above is presented. As in the previous case, results are represented after normalization with respect to the maximum value of the velocity, which, in this case corresponds to the initial condition. As expected, there is a delay between the time at which the pressure gradient is extinguished and the time at which the average velocity vanishes. In the particular situation examined in figure 6b), this delay is about one order of magnitude in t^*. Simulations reported in this figure correspond to a Reynolds number value of 10^6 and a similar behaviour was obtained for smaller values of Re.

Once again, predictions from the volume averaging method are in excellent agreement with those from DNS for all values of t^*, while those from the heuristic model only match DNS results in the extreme values of t^*. Contrary to the previous case, the heuristic model underpredicts the velocity dynamics and this occurs over a time range of roughly three orders of magnitude. Notice that, during the early stage of the process, the values of t^* for which the heuristic model reproduces DNS roughly correspond to those for which

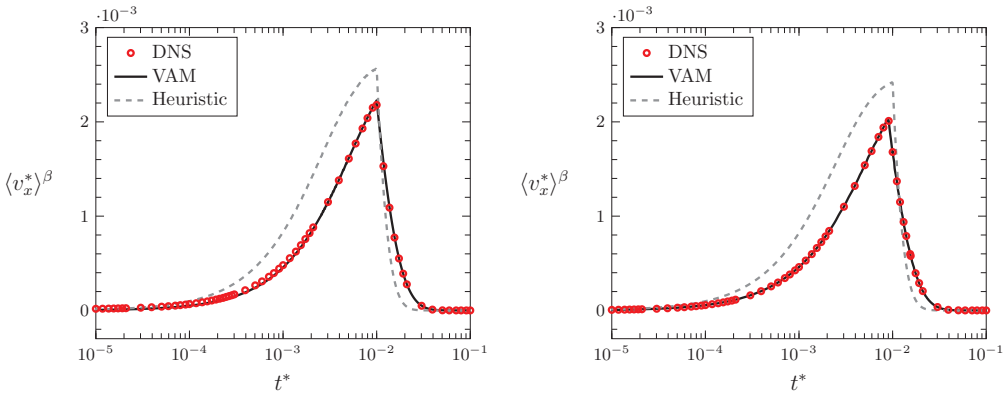

FIGURE 7. Dynamics of the x-component of the macroscale velocity as a response to a macroscopic pressure gradient pulse given by equation (4.7). Results from direct numerical simulations, and from the solution of the macroscale model obtained by the volume averaging method and the heuristic model correspond to a porosity of 0.4 and a) $Re = 10^3$, b) $Re = 10^6$.

the macroscopic pressure gradient is not zero. As a final remark for this case study, it is worth mentioning that the maximum relative error of the predictions from the heuristic model with respect to DNS is about 60%, which is highly contrasting with the one for the predictions of the average model derived here that is below 0.1 %.

4.3. *Case study III: Pressure gradient pulse*

In the two previous cases, the initial flow has been shown to play quite a significant role for the accuracy of the predictions of the macroscale velocity. The remaining case studies deal with situations for which the fluid was initially at rest in the porous medium, while changes of the macroscopic pressure gradient are operated at $t^* > 0$.

In the previous case study, a time delay for the final equilibrium to be reached after the pressure gradient is reduced to zero was highlighted. In the particular case under concern, the interest is to investigate the response to abrupt changes of the macroscopic pressure gradient. Therefore, consider the following dynamics of the macroscopic pressure gradient

$$-\frac{\partial \langle p^* \rangle^\beta}{\partial x^*} = \begin{cases} 0, & t^* \leqslant 0 \\ 1, & 0 < t^* < 10^{-2} \\ 0, & t^* \geqslant 10^{-2} \end{cases} \tag{4.7}$$

In practice, this corresponds to a pressure gradient given as a finite pulse in the porous medium, which could be of interest, from an experimental point of view, for potential measurements of the dynamic apparent permeability. In figure 7 predictions of the dynamics of the dimensionless macroscale velocity are presented for the two values of the Reynolds number, $Re = 10^3$ (figure 7a)) and $Re = 10^6$ (figure 7b)). Notice that the velocity amplitude exhibits a slight decrease as the Reynolds number is increased. In both situations, agreement between DNS and the average model is excellent, whereas the heuristic model overpredicts the velocity for $t^* < 10^{-2}$ and underpredicts it for $t > 10^{-2}$, the largest differences being observed during the first time range. This is consistent with the behaviour observed in the two previous case studies. Indeed, the time period to reach steady state is significantly underpredicted by the heuristic model, compared to DNS or VAM. Finally, it was verified that the results reported in figure 7a) match those obtained

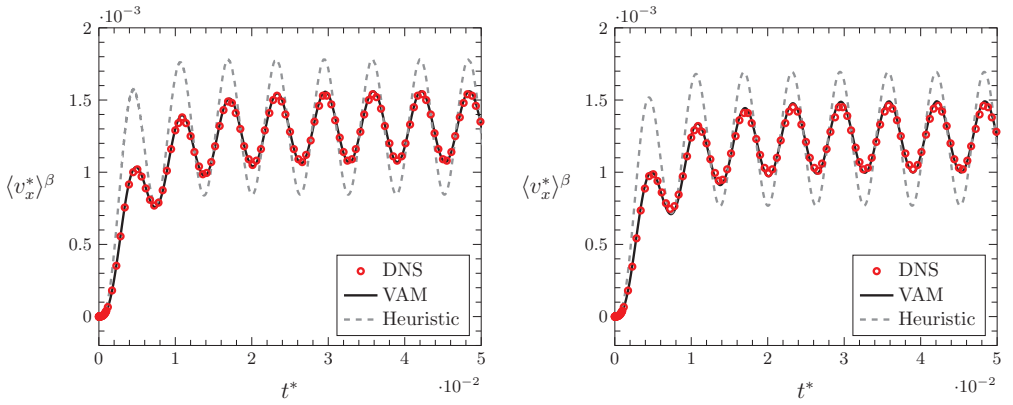

FIGURE 8. Dynamics of the x-component of the macroscale velocity vector, resulting from a response to an oscillatory change in the macroscopic pressure gradient according to equation (4.8). Predictions result from performing direct numerical simulations, from the solution of the macroscale model obtained by the volume averaging method and from the heuristic model. Simulations correspond to a porosity of 0.4 and a) $Re = 10^3$, b) $Re = 10^6$.

under creeping flow conditions. This is consistent with the fact that, for $\varepsilon = 0.4$, H^*_{txx} is not significantly affected by the Reynolds number value up to $Re = 10^4$.

4.4. *Case study IV: Oscillatory pressure gradient*

As a final case study, consider the situation in which the fluid saturating the porous medium was initially at rest and then, at $t^* > 0$, it is subjected to a macroscopic pressure gradient that obeys the following expression,

$$-\frac{\partial \langle p^* \rangle^\beta}{\partial x^*} = 0.5\,[1 - \cos(\omega^* t^*)] \tag{4.8}$$

in which $w^* = 1000$ as in case study II. This situation is also interesting because it corresponds to flow in a porous medium induced by, for example, a peristaltic pump or even a ram pump if the experimental conditions allow a permanent oscillatory pressure gradient.

The resulting predictions of the macroscale velocity are reported in figure 8 following a similar format as the one used in the previous case study. It is observed that the velocity does not exhibit a purely oscillatory dynamics up until $t^* \approx 0.015$ for the two values of Re considered here (namely $Re = 10^3$ and 10^6). In the permanent, but time-dependent regime for $\langle v^*_x \rangle^\beta$ (*i.e.*, for $t^* > 0.015$), the heuristic model is not likely to succeed even at late times, since the model is never reduced to a Darcy-like form. This claim is confirmed by the results shown in figure 8. Although the phase is quite well reproduced, the amplitude of the average velocity is significantly overpredicted by the heuristic model. Although results are not presented here for the sake of brevity, it is observed that, for $\omega^* < 1000$, predictions from this model exhibit a much better performance and reproduce the results from DNS in the permanent regime. This brings to the conclusion that the heuristic model can not be considered as a reliable one except in a specific range of frequencies that are likely to depend on the structure of the porous medium and the frequency spectrum. Conversely, the volume averaged model is in excellent agreement with DNS at all frequencies.

As a matter of overview of the study cases envisaged in this section, it is worth mentioning that the volume averaged model reproduces the results from DNS whatever the

nature of the flow and initial conditions under consideration. This validates the model developed in this work. In these stiff cases, the heuristic model presented poor performance, in general, leading to the conclusion that it is not appropriate.

5. Conclusions

Unsteady flow in porous media is of wide interest for many applications and has been the subject of active work over the past century. However, the available models describing such flows still leave much to be desired as they are either rather heuristic or remain incomplete, in particular regarding the consideration of inertial effects and, to a less extent, the flow initial condition. This motivated the work developed in this article that is dedicated to a formal derivation and analysis of an upscaled model that includes these features for single-phase unsteady flow in rigid and homogeneous periodic porous media. To this end, the pore-scale flow model was upscaled using a short-cut version of the volume averaging method. In this version, the macroscopic forcing was assumed to be spatially-invariant in periodic structures. The resulting model expresses the macroscale velocity as a function of two terms: the first one contains the time rate of change of the convolution between a dynamic apparent permeability tensor and the dynamic macroscopic pressure gradient. The second term accounts for the time-decaying influence of the initial velocity. The convolution product holds a memory effect of the flow history. The unsteady upscaled model is clearly in contradiction with the heuristic model that consists of an *ad hoc* correction to Darcy's law by simply including an acceleration term of the average velocity. Moreover, it generalizes a previously reported model that is only applicable under creeping flow conditions (Lions 1981; Auriault *et al.* 1985; Sheng & Zhou 1988; Zhou & Sheng 1989; Allaire 1992; Mei & Vernescu 2010).

Associated to the macroscale model, ancillary closure problems were derived that allow the determination of the dynamics of the effective coefficients. The dynamic apparent permeability tensor, $\mathbf{H}_t$, was shown to be non-symmetric in general. The irreducible decomposition of $\mathbf{H}_t$ was achieved, showing that the skew-symmetric part is inherent to inertial effects. This further leads to the conclusion that the dynamic permeability in the creeping regime, $\mathbf{K}_t$, is a symmetric tensor. Positiveness was proved for $\mathbf{H}_t$ in the Laplace domain, proving that $\overline{\mathbf{K}}_t$ is a symmetric definite positive tensor although the same is not true for $\overline{\mathbf{H}}_t$.

From the numerical solution of the closure problems, the effective coefficients were predicted in a particular flow situation in simple representations of the porous medium geometry and were found to be functions of time and porosity. After proper normalization, the dependence of the coefficients upon the Reynolds number was collapsed into master curves that were only sensitive to variations in the porosity for the given structure. Although beyond the scope of the present work, further investigation about the extents of this normalization are certainly of interest, as a natural extension to previous works carried out in the creeping regime.

Through a set of stiff flow and initial test conditions, the model was validated by comparison with direct numerical simulations. In all cases, the agreement between the two approaches was excellent, thus justifying the average model. Conversely, the heuristic model was shown to poorly perform predictions of the macroscale velocity.

As a final point of discussion, it is worth mentioning that the requirement of availability of the velocity fields to solve the closure problems, while not mandatory, does not hinder the value of the macroscale model. The only requirements for the predictions of the effective coefficients are the macroscopic forcing and the initial flow field. In fact, beyond the fundamental interest in this formal model, its relevance lies in the potential use for

further upscaling as well as for interpretation of experiments including inertial effects and the influence of the initial condition. Results from this work should serve as a motivation for more theoretical and experimental analyses of unsteady transport phenomena in porous media and many other unsteady processes in hierarchical systems.

Acknowledgements

DL would like to gratefully acknowledge the financial support from the French embassy in Mexico and the IFAL making possible his stay at UAM (CDMX) in November 2017, period during which part of this work was completed. DL is also thankful to UAM for its contribution to the cost of his stay. FJVP would like to thank the University of Bordeaux and ENSAM for providing invited professor positions during spring 2017 and 2018. The authors are thankful to four anonymous reviewers and to G. Allaire for their constructive remarks.

Appendix A.

This appendix is dedicated to a reformulation of the macroscopic momentum equation in the particular situation of creeping flow when the initial condition, $\mathbf{v}_0$, obeys a Stokes model. It is proved that closure problem I is the only problem that needs to be solved.

Since in the case under consideration here, the initial flow and the unsteady flow starting at $t = 0$, characterized by their velocity and pressure fields ($\mathbf{v}_0$, p_0) and ($\mathbf{v}$, p), respectively, obey the Stokes model, a velocity and pressure fields $\mathbf{u} = \mathbf{v} - \mathbf{v}_0$ and $P = p - p_0$ can be defined satisfying the following unsteady Stokes problem within a periodic unit cell

$$\nabla \cdot \mathbf{u} = 0, \quad \text{in } \mathscr{V}_\beta,\ t > 0 \tag{A 1a}$$

$$\rho \frac{\partial \mathbf{u}}{\partial t} = -\nabla \tilde{P} + \mu \nabla^2 \mathbf{u} - \nabla \langle P \rangle^\beta + \rho\,(\mathbf{b} - \mathbf{b}_0), \quad \text{in } \mathscr{V}_\beta,\ t > 0 \tag{A 1b}$$

$$\mathbf{u} = \mathbf{0}, \quad \text{at } \mathscr{A}_{\beta\sigma},\ t \geqslant 0 \tag{A 1c}$$

$$\mathbf{u} = \mathbf{0}, \quad \text{when } t = 0, \quad \text{in } \mathscr{V}_\beta \tag{A 1d}$$

$$\langle \tilde{P} \rangle^\beta = 0, \qquad t > 0 \tag{A 1e}$$

$$\mathbf{u}(\mathbf{r} + \mathbf{l}_i) = \mathbf{u}(\mathbf{r}); \quad \tilde{P}(\mathbf{r} + \mathbf{l}_i) = \tilde{P}(\mathbf{r}), \quad t > 0, \quad i = 1, 2, 3 \tag{A 1f}$$

where $\tilde{P} = \tilde{p} - \tilde{p}_0$ and $\mathbf{b}_0 = \mathbf{b}\,(t = 0)$.

Since the initial condition for the problem for $\mathbf{u}$ and P is zero, the associated macroscopic momentum equation writes (see equation (3.21))

$$\langle \mathbf{u} \rangle = -\frac{1}{\mu} \frac{\partial \mathbf{K}_t}{\partial t} * \cdot \left(\nabla \langle P \rangle^\beta - \rho\,(\mathbf{b} - \mathbf{b}_0) \right), \quad t > 0 \tag{A 2}$$

where $\mathbf{K}_t$ is the dynamic permeability in the absence of inertia. In addition, at the macroscale, the initial steady flow obeys a Darcy-like equation, *i.e.*

$$\langle \mathbf{v}_0 \rangle = -\frac{\mathbf{K}}{\mu} \cdot \left(\nabla \langle p_0 \rangle^\beta - \rho \mathbf{b}_0 \right), \quad t = 0 \tag{A 3}$$

where $\mathbf{K}$ is the intrinsic permeability of the medium corresponding to $\mathbf{K}_t$ at sufficiently large times. When $\mathbf{u}$ and P are replaced by their expressions in terms of $\mathbf{v}$, $\mathbf{v}_0$, p and p_0

in equation (A 2), the unsteady macroscopic form of the momentum equation in the case under study is given by

$$\langle \mathbf{v} \rangle = -\frac{1}{\mu}\frac{\partial \mathbf{K}_t}{\partial t} * \cdot \left(\nabla \langle p \rangle^{\beta} - \rho \mathbf{b}\right) - \frac{1}{\mu}\left(\mathbf{K} - \mathbf{K}_t\right) \cdot \left(\nabla \langle p_0 \rangle^{\beta} - \rho \mathbf{b}_0\right), \quad t > 0 \tag{A 4}$$

or, equivalently

$$\langle \mathbf{v} \rangle = -\frac{1}{\mu}\frac{\partial \mathbf{K}_t}{\partial t} * \cdot \left(\nabla \langle p \rangle^{\beta} - \rho \mathbf{b}\right) + \left(\mathbf{I} - \mathbf{K}_t \cdot \mathbf{K}^{-1}\right) \cdot \langle \mathbf{v}_0 \rangle, \quad t > 0 \tag{A 5}$$

This clearly shows that, in this particular case, the only closure problem that needs to be solved is *Problem I*, yielding $\mathbf{K}_t$ (and $\mathbf{K}$ at sufficiently long time).

REFERENCES

Abderahmane, K., Khalifa, O. A., Wahyudi, I. & Thomas, P. 2002 New extension of Darcy's law to unsteady flows. *Soils and Foundations* **42**, 53–63.

Achdou, Y. & Avellaneda, M. 1992 Influence of pore roughness and pore-size dispersion in estimating the permeability of a porous medium from electrical measurements. *Physics of Fluids A: Fluid Dynamics* **4** (12), 2651–2673.

Agnaou, M., Lasseux, D. & Ahmadi, A. 2016 From steady to unsteady laminar flow in model porous structures: An investigation of the first Hopf bifurcation. *Computers and Fluids* **136**, 67–82.

Allaire, G. 1992 *Progress in partial differential equations: calculus of variations, applications*, chap. Homogenization of the unsteady Stokes equations in porous media. Longman Scientific & Technical.

Auriault, J. L. 1980 Dynamic behaviour of a porous medium saturated by a Newtonian fluid. *International Journal of Engineering Science* **18** (6), 775–785.

Auriault, J. L. 1999 Comments on the paper 'Local and global transitions to chaos and hysteresis in a porous layer heated from below', by P. Vadasz. *Transport in Porous Media* **37**, 247–249.

Auriault, J. L., Borne, L. & Chambon, R. 1985 Dynamics of porous saturated media, checking of the generalized law of Darcy. *The Journal of the Acoustical Society of America* **77** (5), 1641–1650.

Auriault, J. L., Boutin, C. & Geindreau, C. 2009 *Homogenization of Coupled Phenomena in Heterogenous Media*. ISTE LTD.

Balhoff, M., Mikelić, A. & Wheeler, M. F. 2010 Polynomial filtration laws for low reynolds number flows through porous media. *Transport in Porous Media* **81** (1), 35–60.

Barrere, J., Gipouloux, O. & Whitaker, S. 1992 On the closure problem for Darcy's law. *Transport in Porous Media* **7** (3), 209–222.

Biot, M. A. 1956*a* Theory of propagation of elastic waves in a fluid-saturated porous solid. I. Low-frequency range. *The Journal of the Acoustical Society of America* **28** (2), 168–178.

Biot, M. A. 1956*b* Theory of propagation of elastic waves in a fluid-saturated porous solid. II. Higher frequency range. *The Journal of the Acoustical Society of America* **28** (2), 179–191.

Bories, S., Mojtabi, A., Prat, M. & Quintard, M. 2008 Transferts de chaleur dans les milieux poreux - Conduction, convection, rayonnement. *Techniques de l'Ingénieur* **BE 8250**, 1–22.

Bourgeat, A., Marušić-Paloka, E. & Mikelić, A. 1996 Weak nonlinear corrections for Darcy's law. *Mathematical Models and Methods in Applied Sciences* **06** (08), 1143–1155.

Breugem, W. P., Boersma, B. J. & Uittenbogaard, R. E. 2006 The influence of wall permeability on turbulent channel flow. *Journal of Fluid Mechanics* **562**, 35–72.

Burcharth, H. F. & Andersen, O. H. 1995 On the one-dimensional steady and unsteady porous flow equations. *Coastal Engineering* **24**, 233–257.

Chapman, A. M. & Higdon, J. J. L. 1992 Oscillatory stokes flow in periodic porous media. *Physics of Fluids A: Fluid Dynamics* **4** (10), 2099–2116.

Charlaix, E., Kushnick, A. P. & Stokes, J. P. 1988 Experimental study of dynamic permeability in porous media. *Physical Review Letters* **61** (14), 1595–1598.

Cortis, A., Smeulders, D. M. J., Guermond, J. L. & Lafarge, D. 2003 Influence of pore roughness on high-frequency permeability. *Physics of Fluids* **15** (6), 1766.

Corvaro, S., Mancinelli, A., Brocchini, M., Seta, E. & Lorenzoni, C. 2010 On the wave damping due to a permeable seabed. *Coastal Engineering* **57**, 1029–1041.

Cushman, J. H., Bennethum, L. S. & Hu, B. X. 2002 A primer on upscaling tools for porous media. *Advances in Water Resources* **25** (8–12), 1043 – 1067.

Dogru, A. H., Alexander, W. & Panton, R. L. 1978 Numerical solution of unsteady flow problems in porous media by spline functions. *Journal of Hydrology* **38**, 179–195.

Gray, W.G. 1975 A derivation of the equations for multiphase transport. *Chemical Engineering Science* **30**, 229–233.

Gray, W. G. & Miller, C. T. 2014 *Introduction to the Thermodynamically Constrained Averaging Theory for Porous Medium Systems*. Springer International Publishing.

Hall, K. R., Smith, G. M. & Turcke, D. J. 1995 Comparison of oscillatory and stationary flow through porous media. *Coastal Engineering* **24**, 217–232.

Hill, A. A. & Straughan, B. 2008 Poiseuille flow in a fluid overlying a porous medium. *Journal of Fluid Mechanics* **603**, 137–149.

Hill, A. A. & Straughan, B. 2009 Poiseuille flow in a fluid overlying a highly porous material. *Advances in Water Resources* **32**, 1609–1614.

Howes, F.A. & Whitaker, S. 1985 The spatial averaging theorem revisited. *Chemical Engineering Science* **40**, 1387–1392.

Jin, Y. & Kuznetsov, A. V. 2017 Turbulence modeling for flows in wall bounded porous media: An analysis based on direct numerical simulations. *Physics of Fluids* **29** (4), 045102.

Johnson, D. L. 1989 Scaling function for dynamic permeability in porous media. *Physical Review Letters* **63** (5), 580.

Johnson, D. L., Koplik, J. & Dashen, R. 1987 Theory of dynamic permeability and tortuosity in fluid-saturated porous media. *Journal of Fluid Mechanics* **176**, 379–402.

Kuznetsov, A. V. & Nield, D. A. 2006 Forced convection with laminar pulsating flow in a saturated porous channel or tube. *Transport in Porous Media* **65**, 505–523.

Lasseux, D., Abbasian-Arani, A. A. & Ahmadi, A. 2011 On the stationary macroscopic inertial effects for one phase flow in ordered and disordered porous media. *Physics of Fluids* **23**, 073103.

Lasseux, D. & Valdés-Parada, F.J. 2017 Symmetry properties of macroscopic transport coefficients in porous media. *Physics of Fluids* **29**, 043303.

Laushey, L. M. & Popat, L. V. 1968 Darcy's law during unsteady flow. In *Ground Water: General Assembly of Bern* (ed. L. J. Tison), pp. 284–299. International Union of Geodesy and Geophysics (IUGG) and International Association of Scientific Hydrology (IASH), Boulder, http://iahs.info/ redbooks/a077/077028.pdf (1968).

Lévy, T. 1979 Propagation of waves in a fluid-saturated porous elastic solid. *International Journal of Engineering Science* **17** (9), 1005–1014.

Lions, J. L. 1981 *Some methods in the mathematical analysis of systems and their control*. Gordon and Breach.

Lions, P. L. & Masmoudi, N. 2005 Homogenization of the Euler system in a 2D porous medium. *Journal de Mathématiques Pures et Appliquées* **84**, 1–20.

Marušić-Paloka, E. & Mikelić, A. 2000 The derivation of a nonlinear filtration law including the inertia effects via homogenization. *Nonlinear Analysis: Theory, Methods & Applications* **42** (1), 97–137.

Masmoudi, N. 1998 The Euler limit of the Navier-Stokes equations, and rotating fluids with boundary. *Archive for Rational Mechanics and Analysis* **142**, 375–394.

Masmoudi, N. 2002 Homogenization of the compressible Navier-Stokes equations in a porous medium. *ESAIM: Control, Optimisation and Calculus of Variations* **8**, 885–906.

Mei, C. C. & Vernescu, B. 2010 *Homogenization methods for multiscale mechanics*. World Scientific.

Mikelić, A. 1994 Mathematical derivation of the Darcy-type law with memory effects, governing transient flow through porous medium. *Glasnik Matematicki* **29** (49), 57–77.

Nield, D. A. & Bejan, A. 2013 *Convection in porous media*. New-York: Springer.

Polubarinova-Kochina, P. Ya. 1962 *Theory of ground water movement (Translated from the Russian edition by J. M. Roger de Wiest)*. Princeton: Princeton University Press.

Rajagopal, K. R. 2007 On a hierarchy of approximate models for flows of incompressible fluids through porous solids. *Mathematical Models and Methods in Applied Sciences* **17**, 215–252.

Sahimi, M. 2011 *Flow and transport in porous media and fractured rock. From classical methods to modern approaches*. Weinheim: Wiley-CH.

Sanchez-Palencia, E. 1980 Lecture Notes in Physics. In *Non-homogeneous media and vibration theory*. Berlin: Springer-Verlag.

Sheng, P. & Zhou, M.-Y. 1988 Dynamic permeability in porous media. *Physical Review Letters* **61** (14), 1591–1594.

Slattery, J. C. 1999 *Advanced Transport Phenomena*. Cambridge, UK: Cambridge University Press.

Smeulders, D. M. J., Eggels, R. L. G. M. & Dongen, M. E. H. Van 1992 Dynamic permeability: reformulation of theory and new experimental and numerical data. *Journal of Fluid Mechanics* **245**, 211–227.

Sollitt, C. K. & Cross, R. H. 1972 Wave transmission through permeable breakwaters. In *Proceedings of 13th Coastal Engineering Conference, ASCE, vol. 3, pp. 1827–1846*.

Teng, H. & Zhao, T. S. 2000 An extension of Darcy's law to non-Stokes flow in porous media. *Chemical Engineering Science* **55**, 2737–2755.

Tilton, N. & Cortelezzi, L. 2008 Linear stability analysis of pressure-driven flows in channels with porous walls. *Journal of Fluid Mechanics* **604**, 411–445.

Truesdell, C. & Toupin, R. 1960 *The Classical Field Theories*. New-York: Springer Verlag.

Vadasz, P. 1999 Local and global transitions to chaos and hysteresis in a porous layer heated from below. *Transport in Porous Media* **37**, 213–235.

Whitaker, S. 1996 The Forchheimer equation: a theoretical development. *Transport in Porous Media* **25**, 27–61.

Whitaker, S. 1999 *The Method of Volume Averaging*. Kluwer Academic Publishers.

Wood, B.D. & Valdés-Parada, F.J. 2013 Volume averaging: Local and nonlocal closures using a Green's function approach. *Advances in Water Resources* **51**, 139–167.

Zhou, M.-Y. & Sheng, P. 1989 First-principles calculations of dynamic permeability in porous media. *Physical Review B* **39** (16), 12027–12039.

Zhu, T., Waluga, C., Wohlmuth, B. & Manhart, M. 2014 A study of the time constant in unsteady porous media flow using direct numerical simulation. *Transport in Porous Media* **104**, 161–179.